

Computational neuroscience: biophysics - Lecture 7

EPFL, 2024

Connections



Lecture Overview

- Scope
- Approaches
- Applications



Lecture Overview

- Scope
- Approaches
- Applications



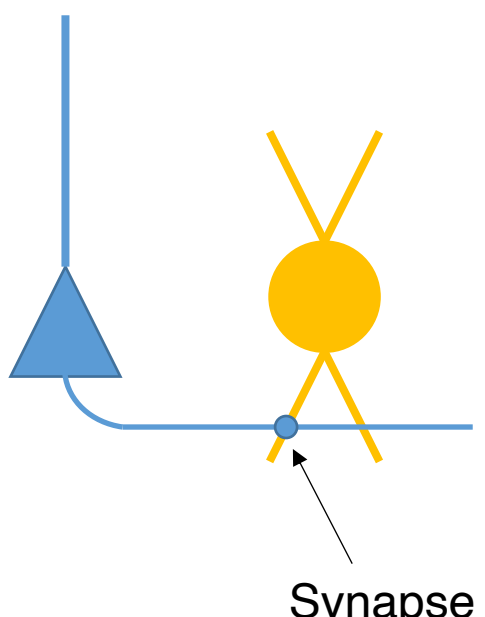
Lecture Overview

- Scope
 - Analyze connections
 - Experimental methods
- Approaches
- Applications



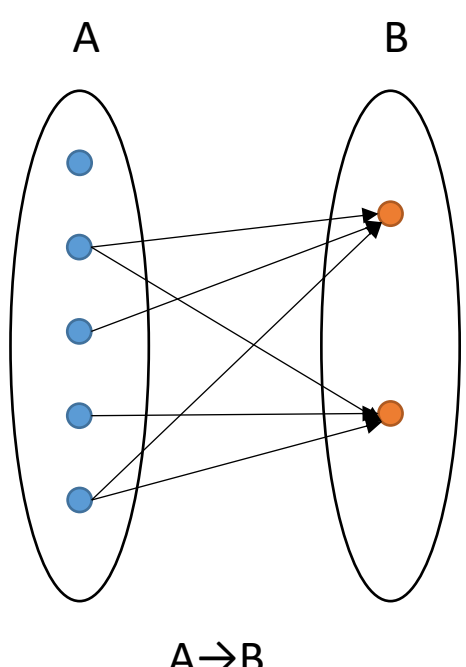
Connections

An instance of the pathway PC -> INT





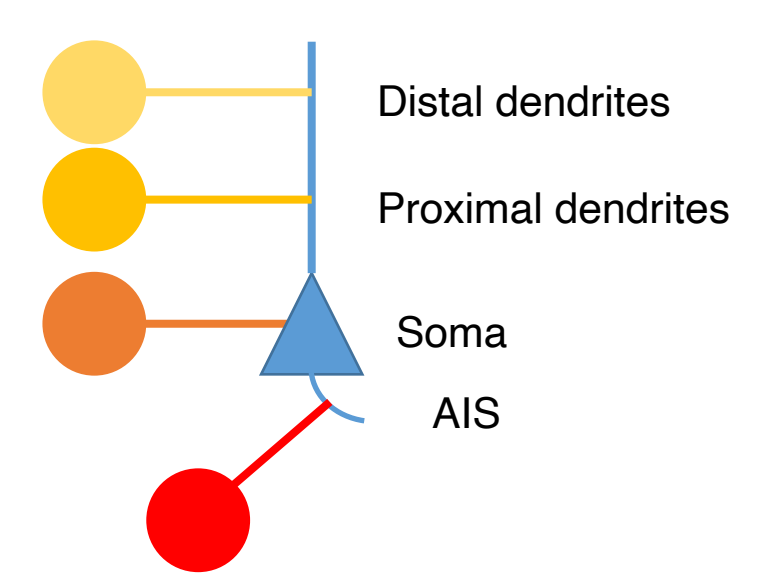


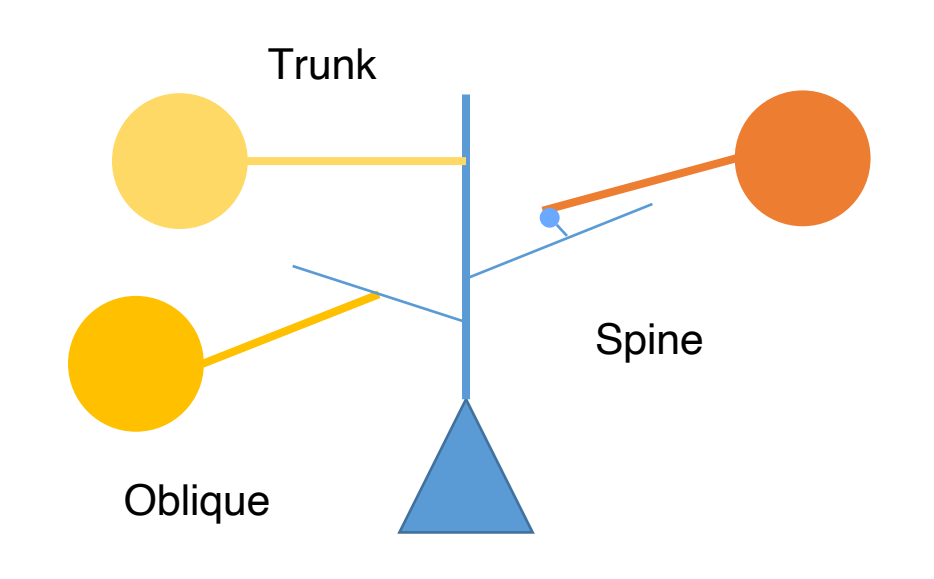


Λ	\	D
А	7	D

Pre\Post	A	В
Α	0	1
В	0	0

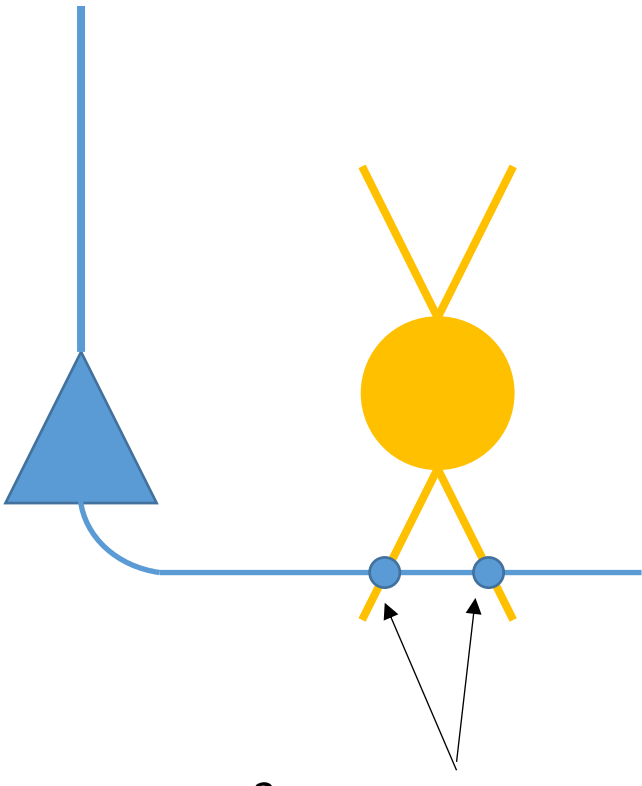
Cell targeting







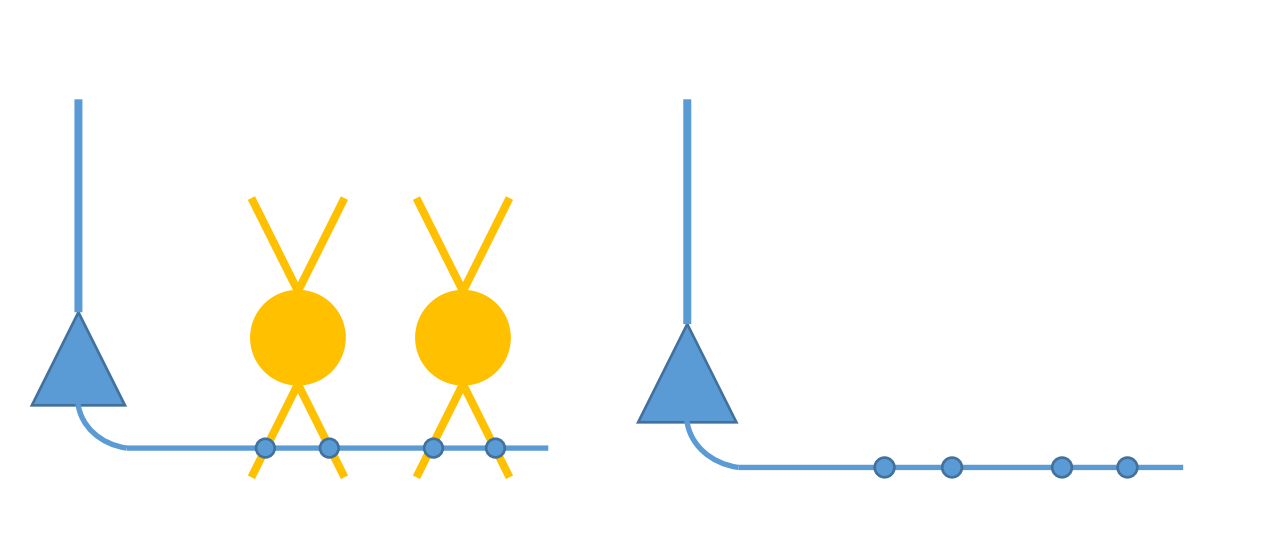
Number of synapses per connection

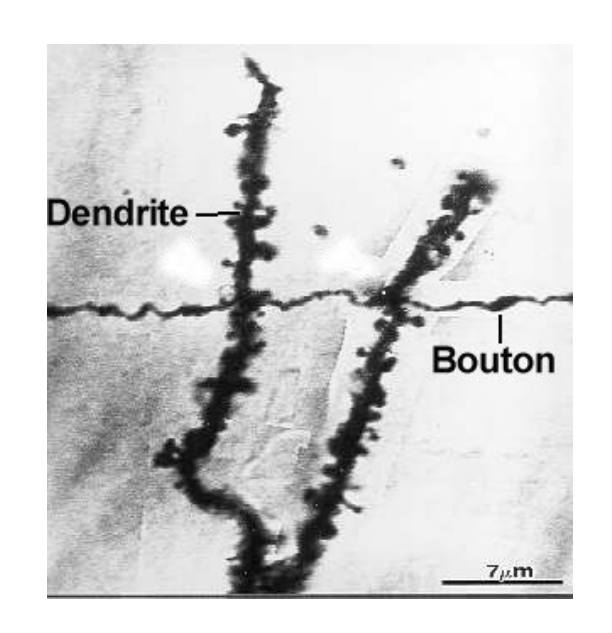


2 synapses per connection



Bouton density



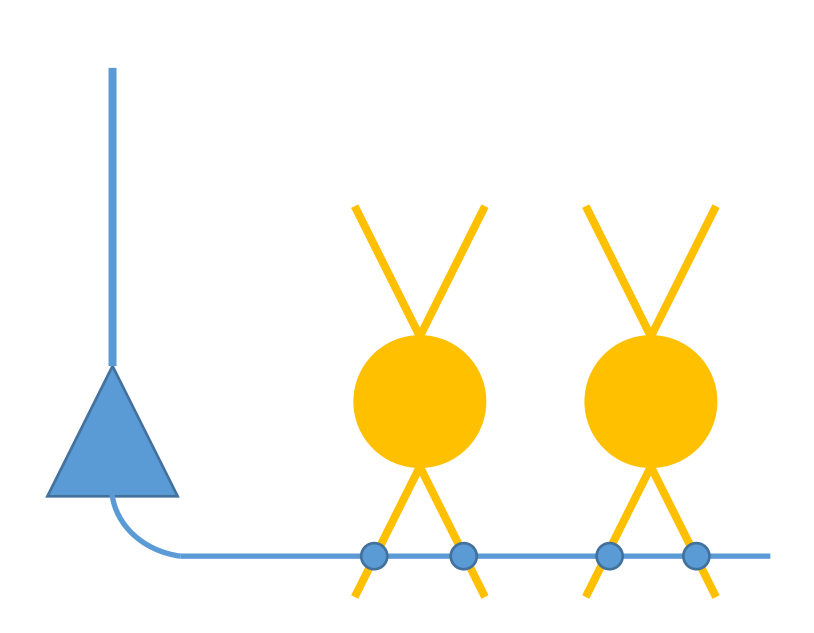


Bouton density = number of boutons / axon length

/ 100 μ m or / μ m

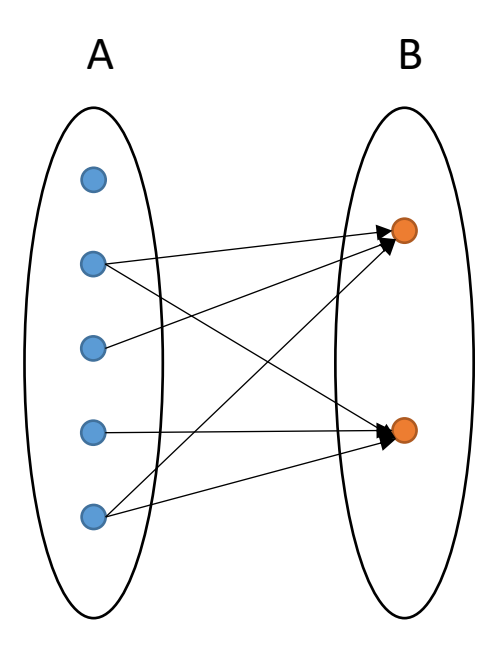


Divergence



1 PC contacts 2 interneurons

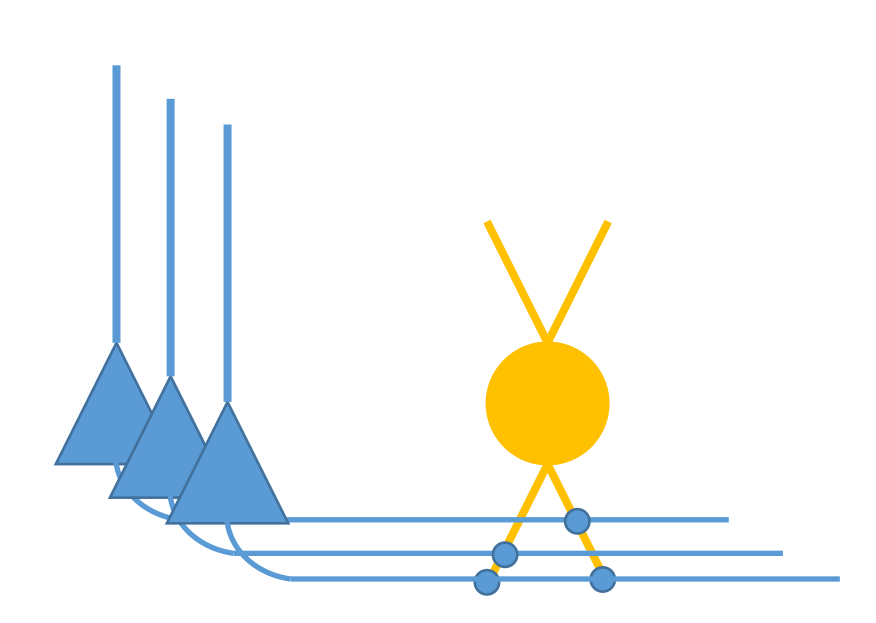




Divergence($A \rightarrow B$)

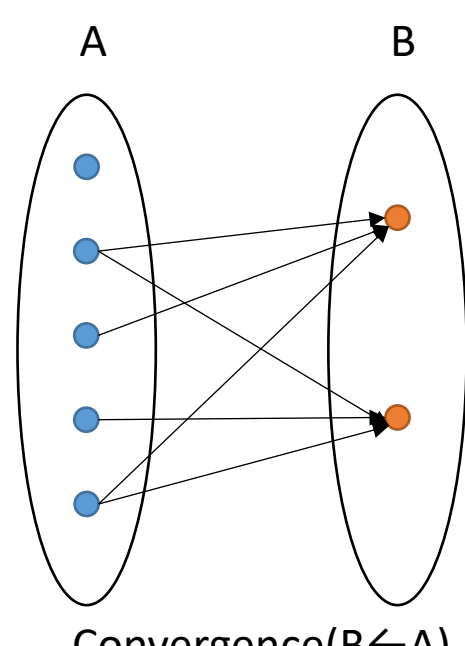
Pre\Post	Α	В
Α	0	1.2
В	0	0

Convergence



1 INT is contacted by 3 PCs

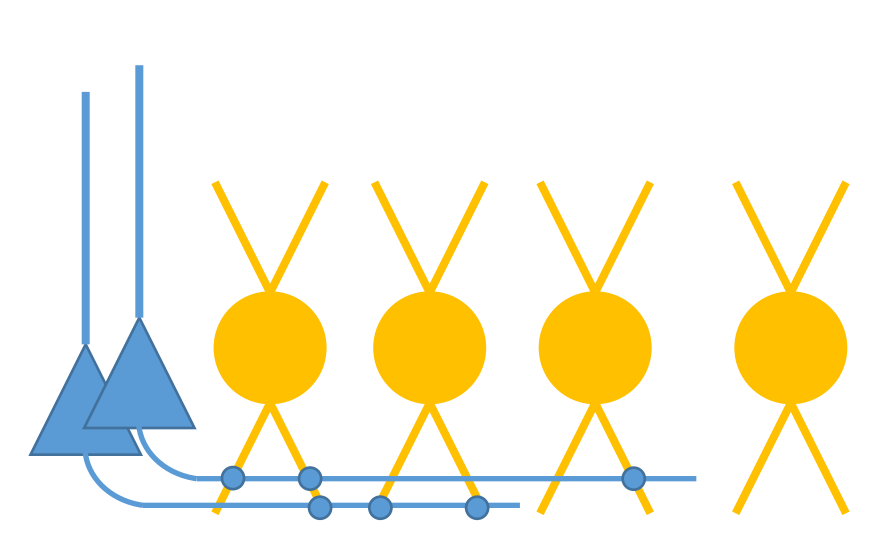




Convergence($B \leftarrow A$)

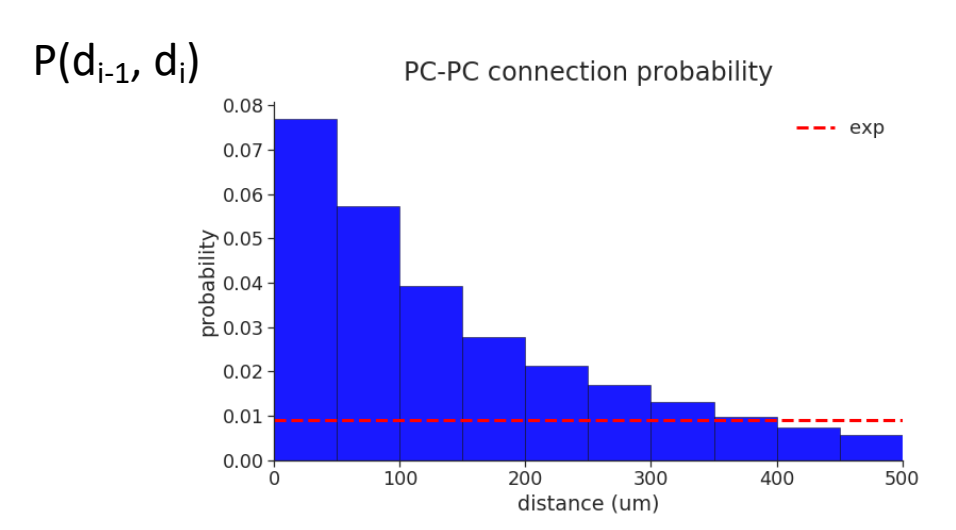
Pre\Post	Α	В
Α	0	3
В	0	0

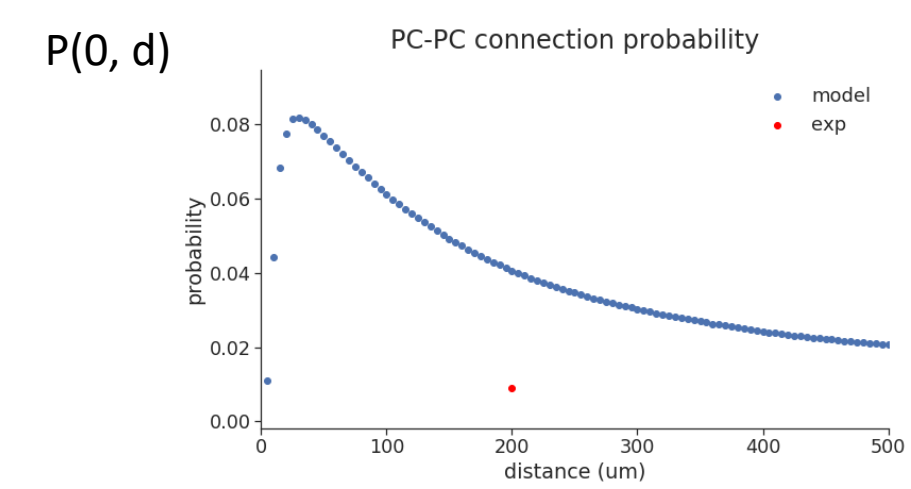
Connection probability



connected pairs / all pairs 4 / 8 = 0.5 or 50%





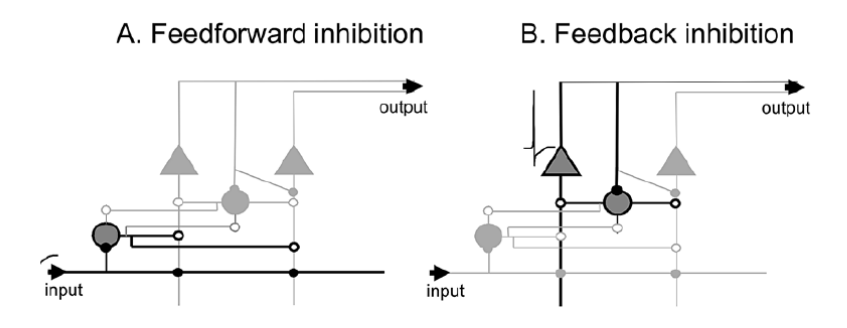


Higher-order descriptors

- Local connectivity patterns
- Graph theory
- Topography of long-range projections



Local connectivity patterns



C. Recurrent excitation

output output input

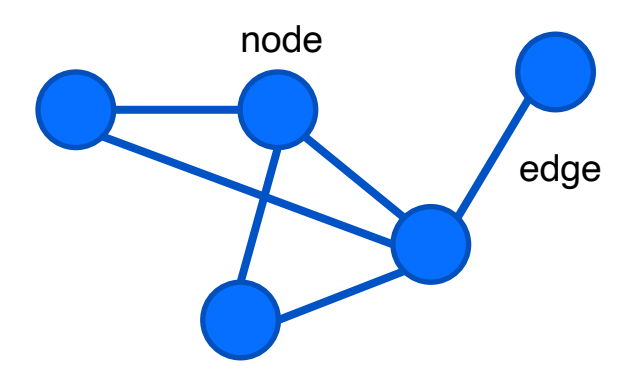
Figure 8-1. Basic local circuit interactions. A. Feedforward inhibition. Axon collaterals from excitatory afferent fibers contact local interneurons. The additional synaptic delay compared to direct afferent excitation onto principal cells provides a time-dependent sequence of excitation and inhibition from single afferent inputs. B. Feedback inhibition. Axon collaterals from local principal cells contact local interneurons, providing a period of inhibition of principal cell activity following the generation of an output. Interneuron populations involved in A and B are not always mutually exclusive.

C. Recurrent excitation. Axon collaterals from local principal cells also contact other local principal cells, providing an excitatory mechanism for concerted, temporally coordinated population output. D. Mutual inhibition. Some interneuron subtypes contact other interneurons as well as principal cells, and some interneurons contact other interneurons exclusively. This pattern of connectivity can serve to impart spatiotemporally coordinated patterns of excitation and inhibition in the local circuit leading to rhythm generation. Filled circles, excitatory synapses; open circles, inhibitory synapses.

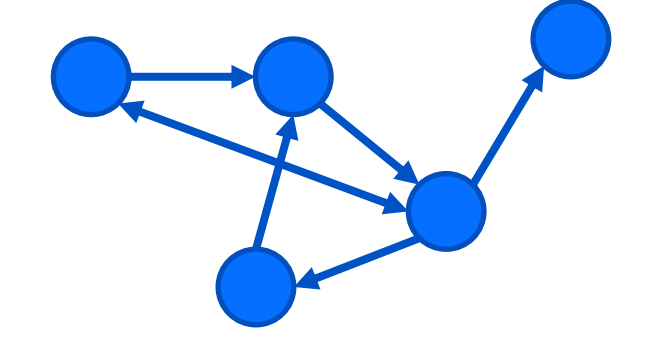
D. Mutual inhibition



Graph theory



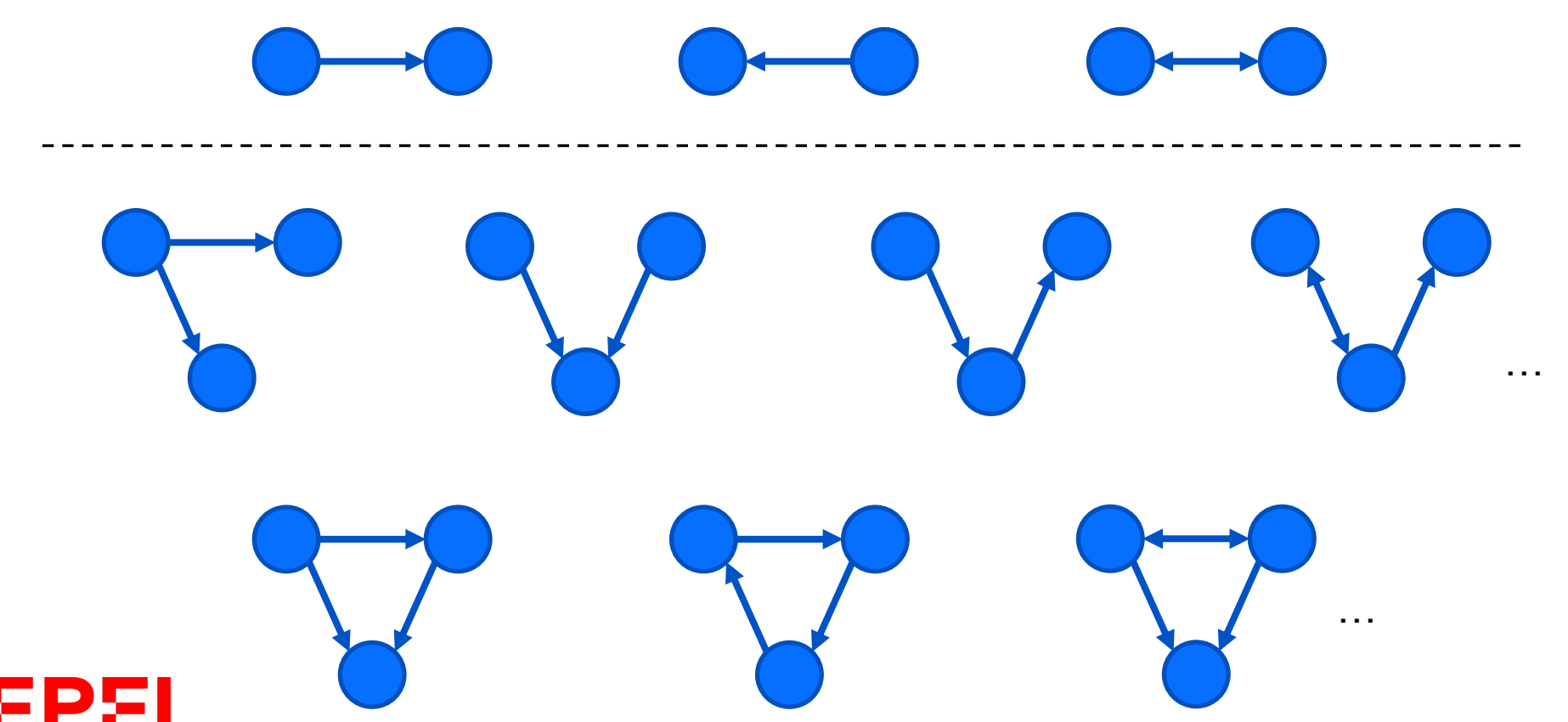
Undirected graph

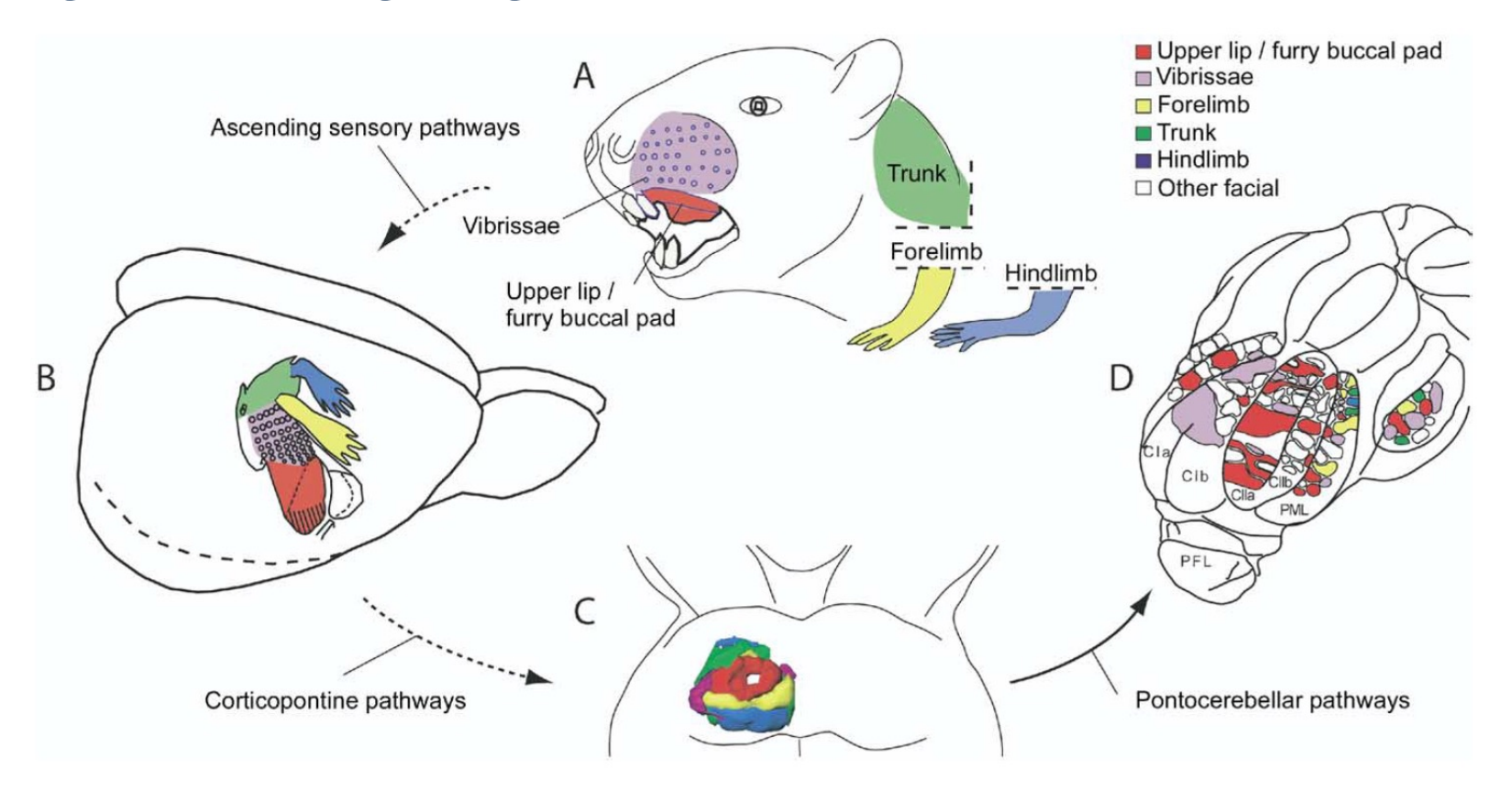


Directed graph



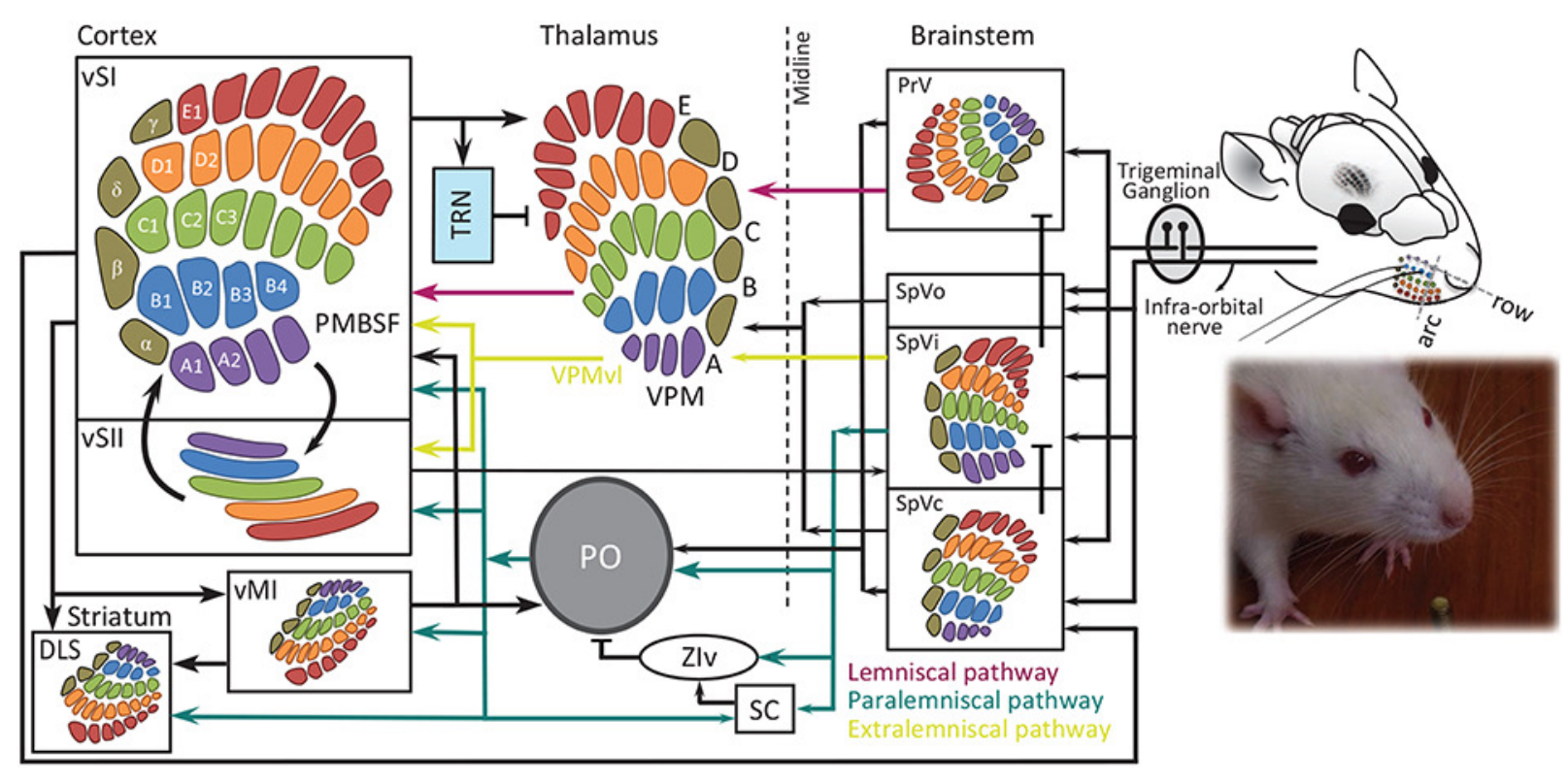
Motifs



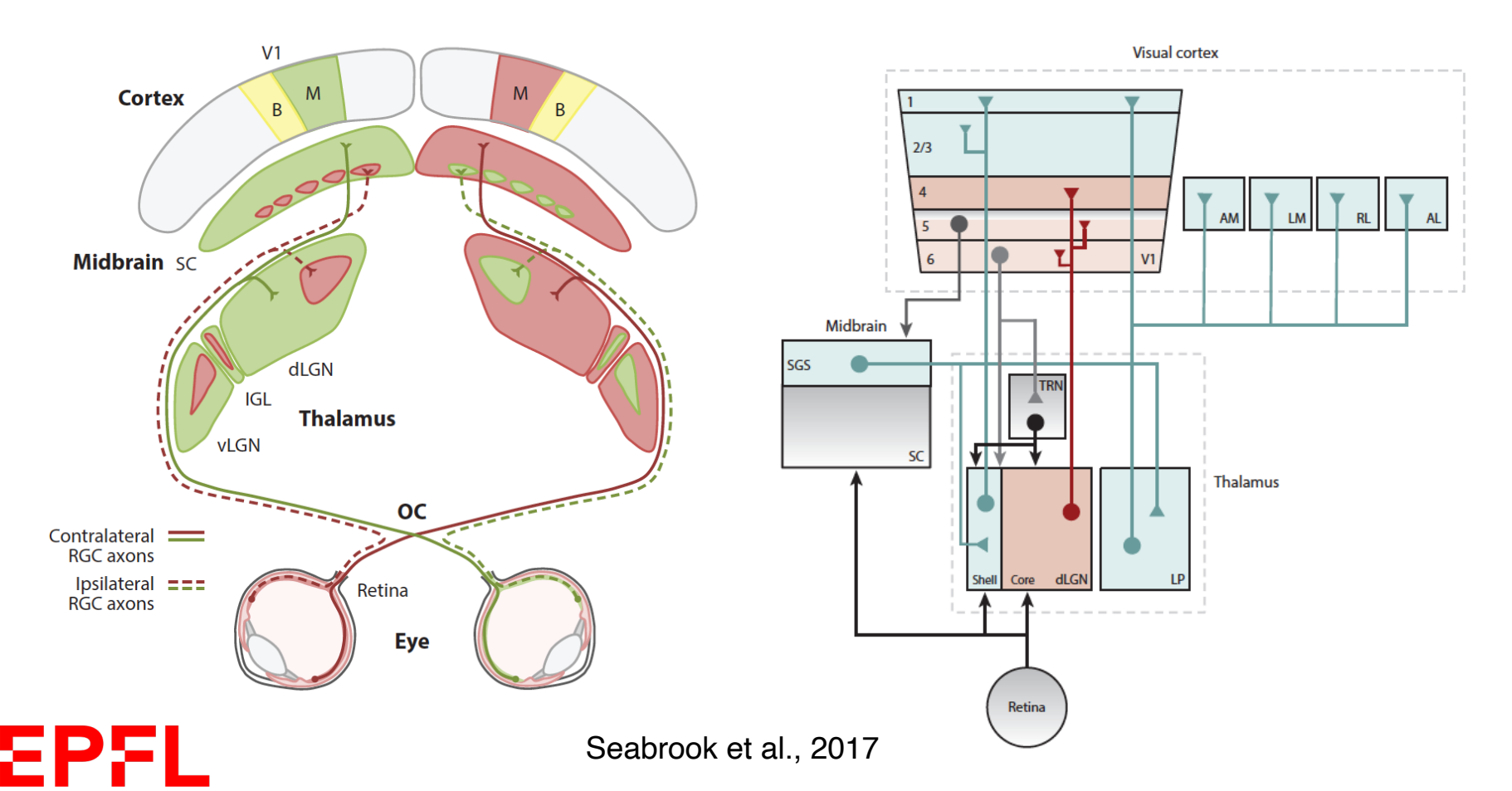


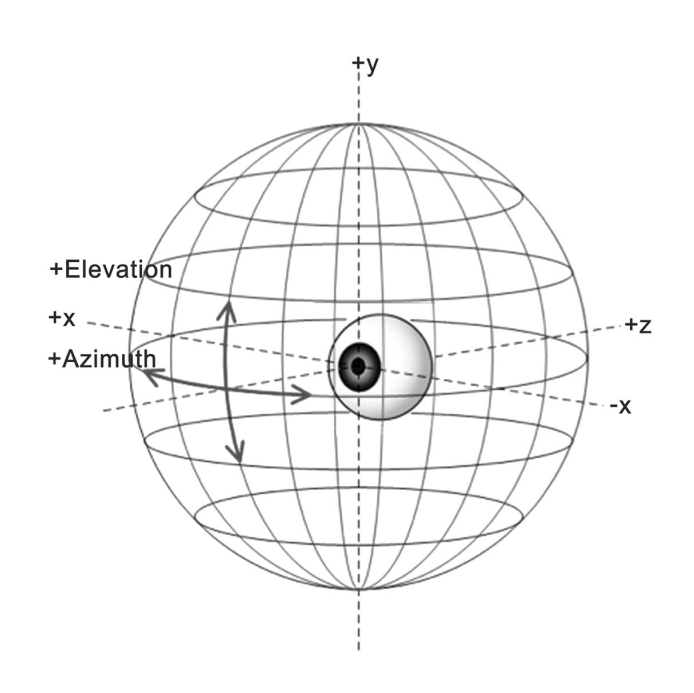


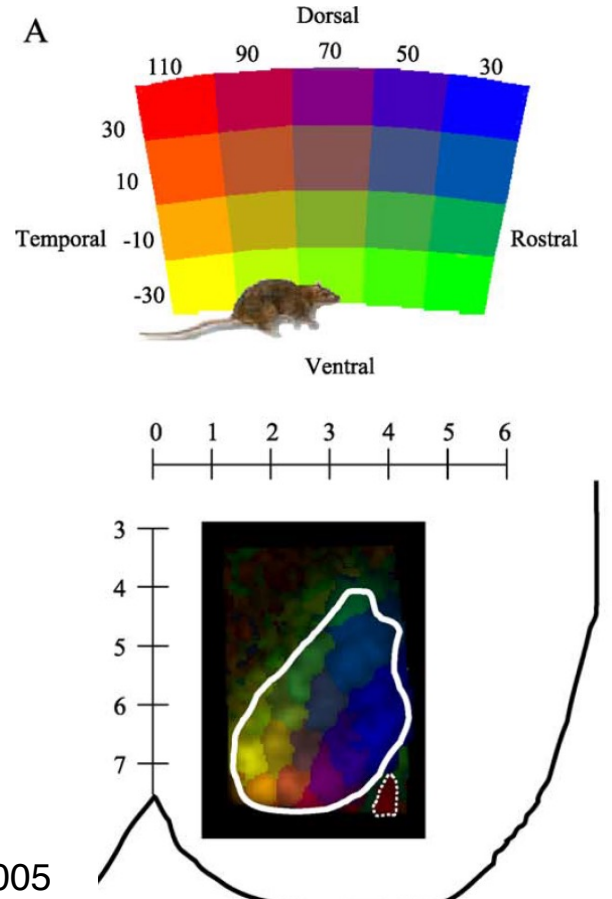
Bjaalie et al., 2005





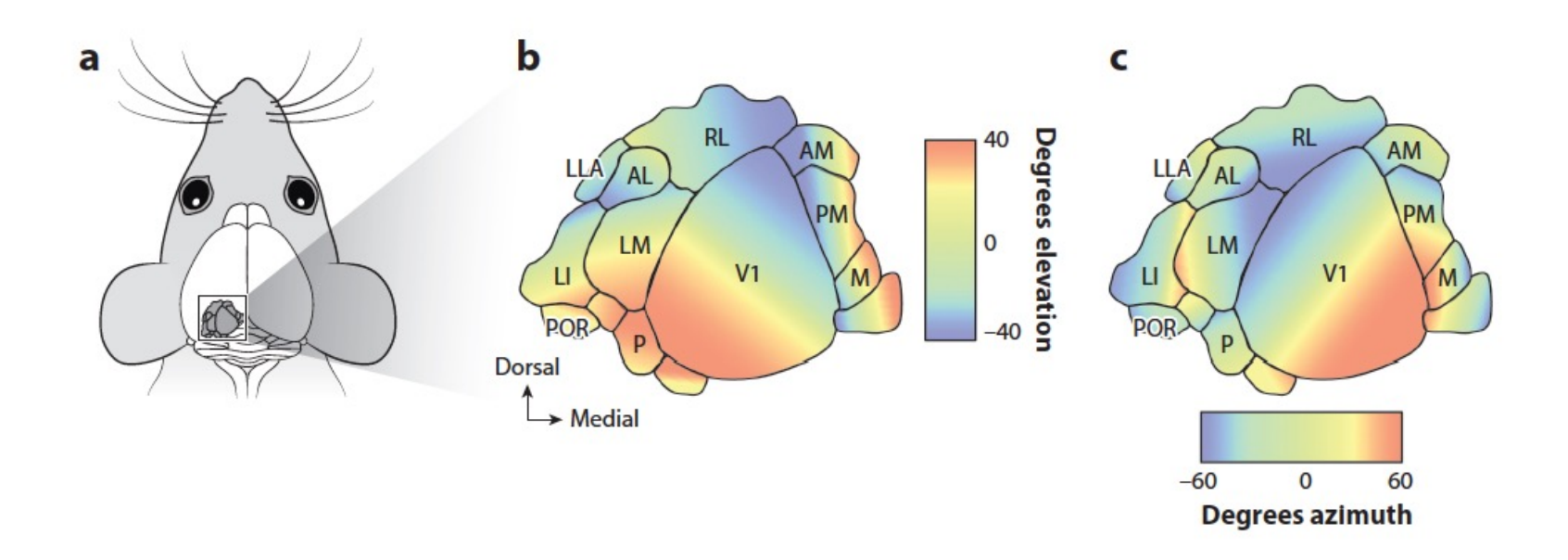




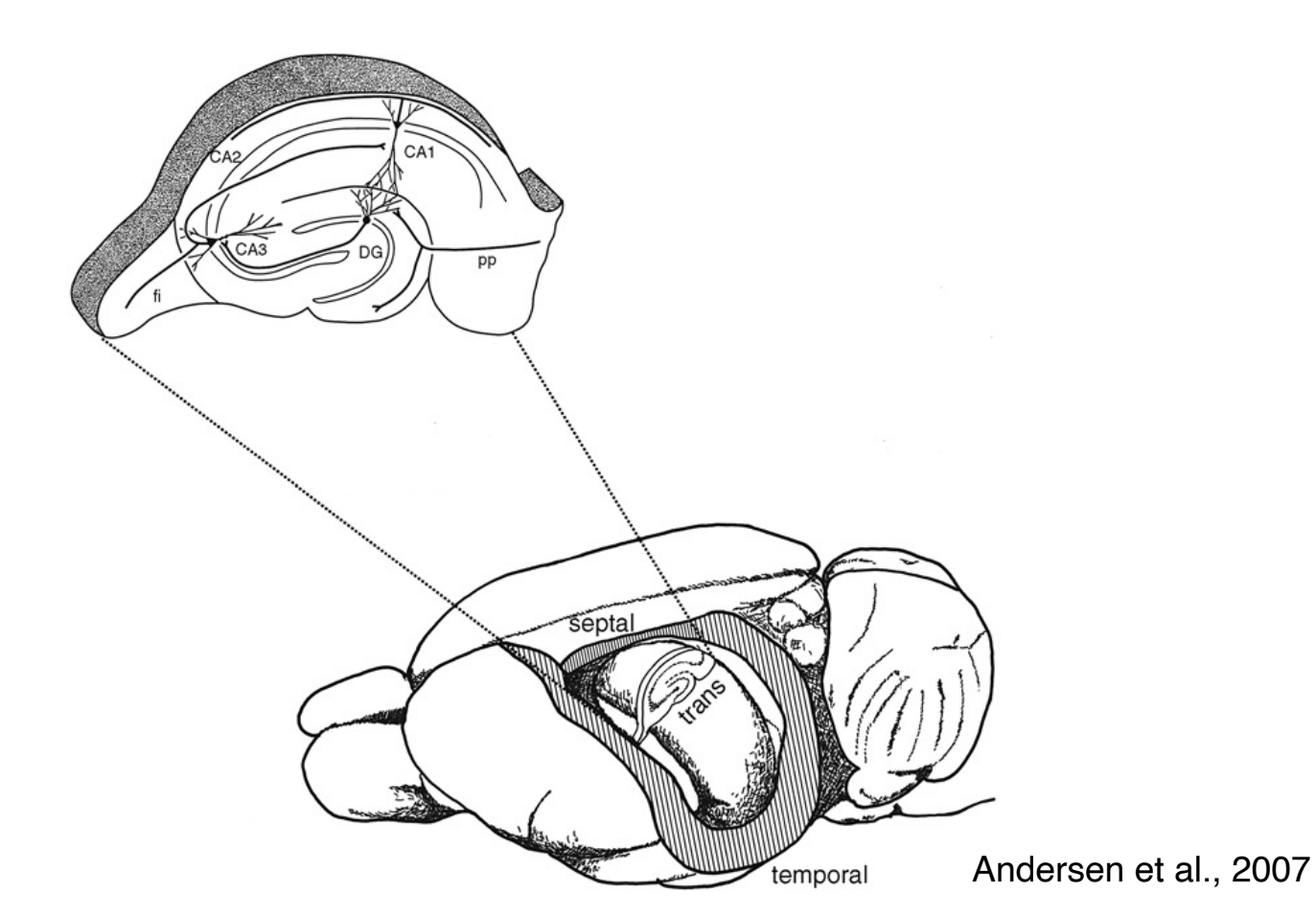




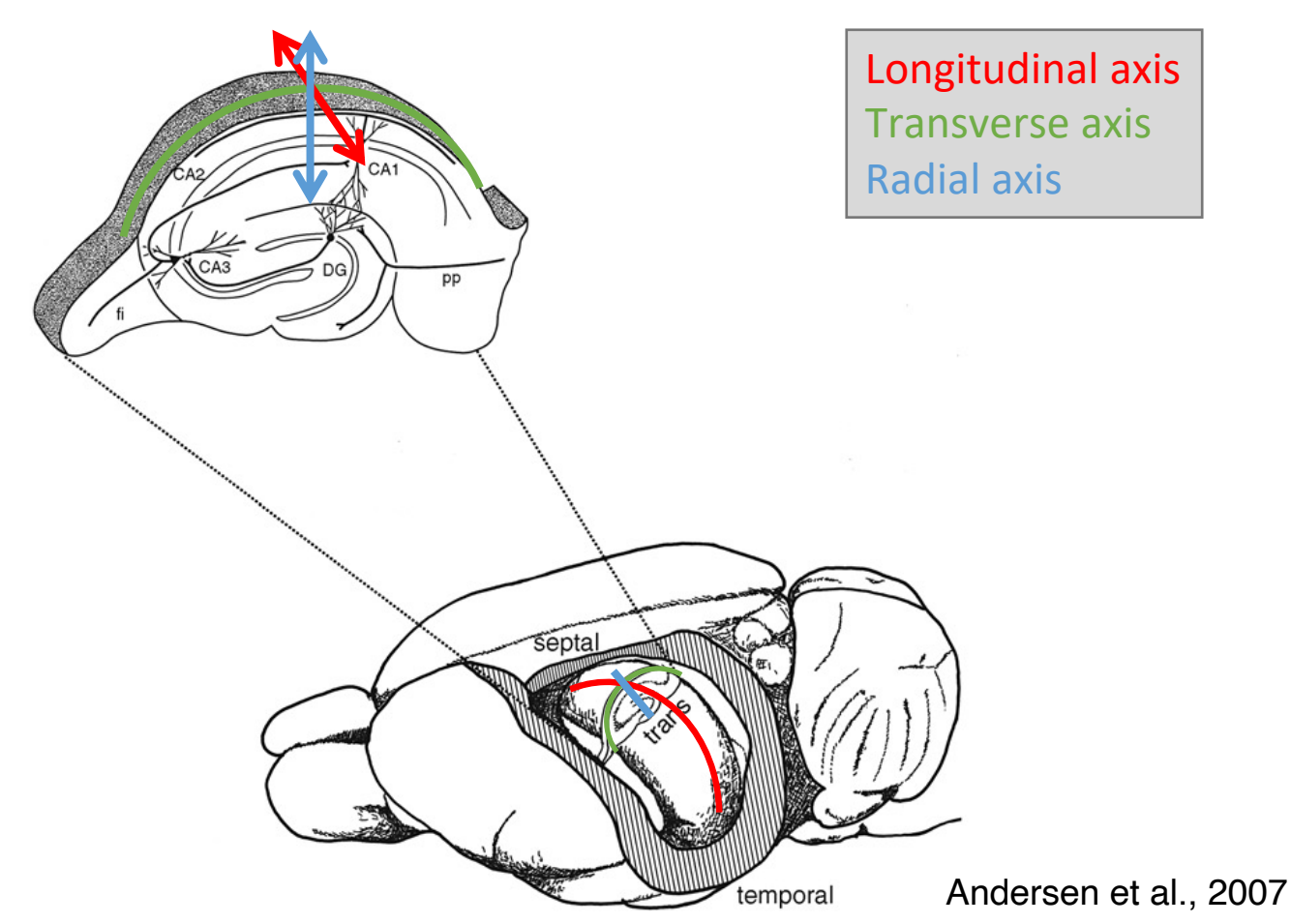
Gias et al., 2005



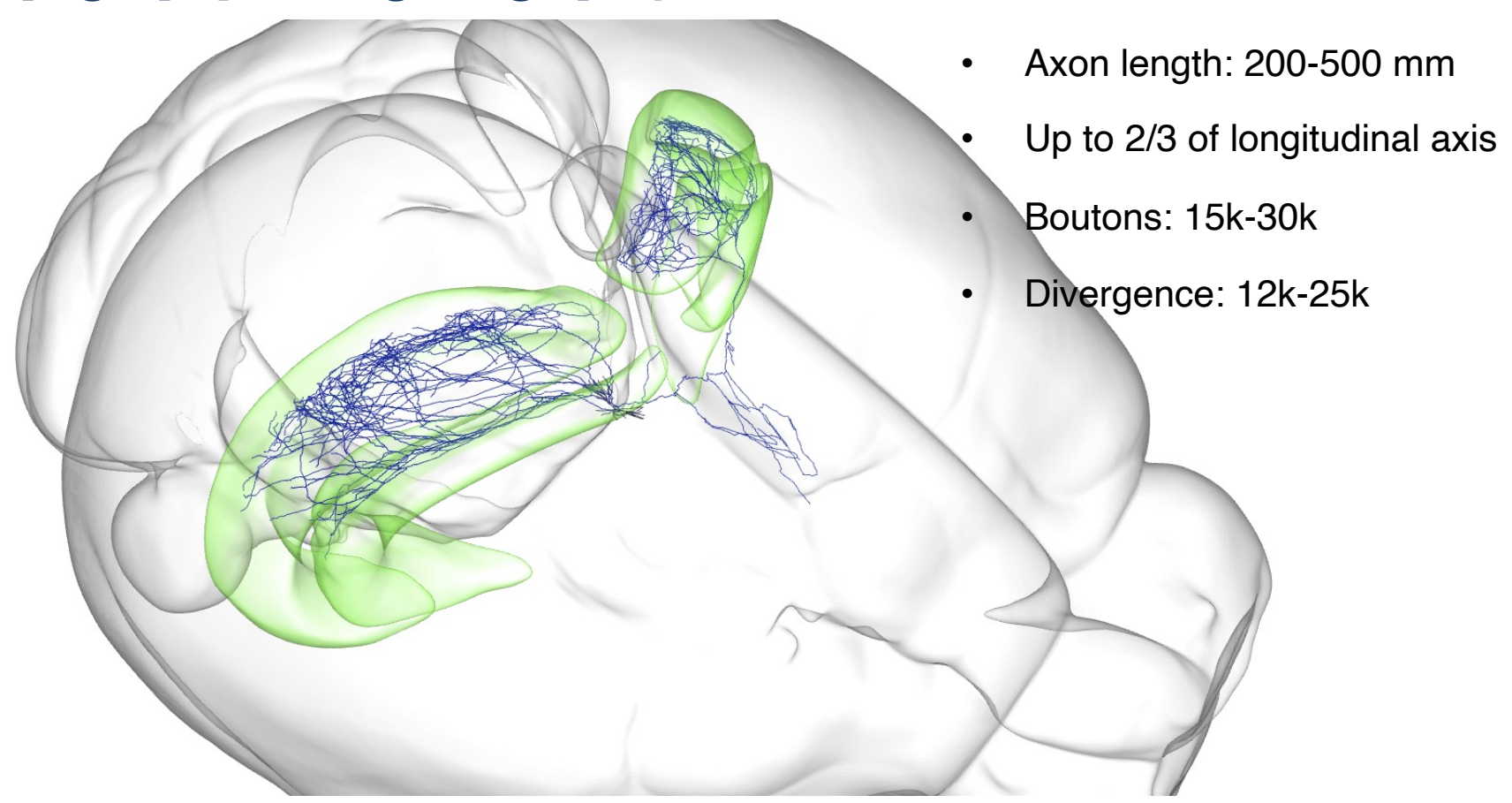






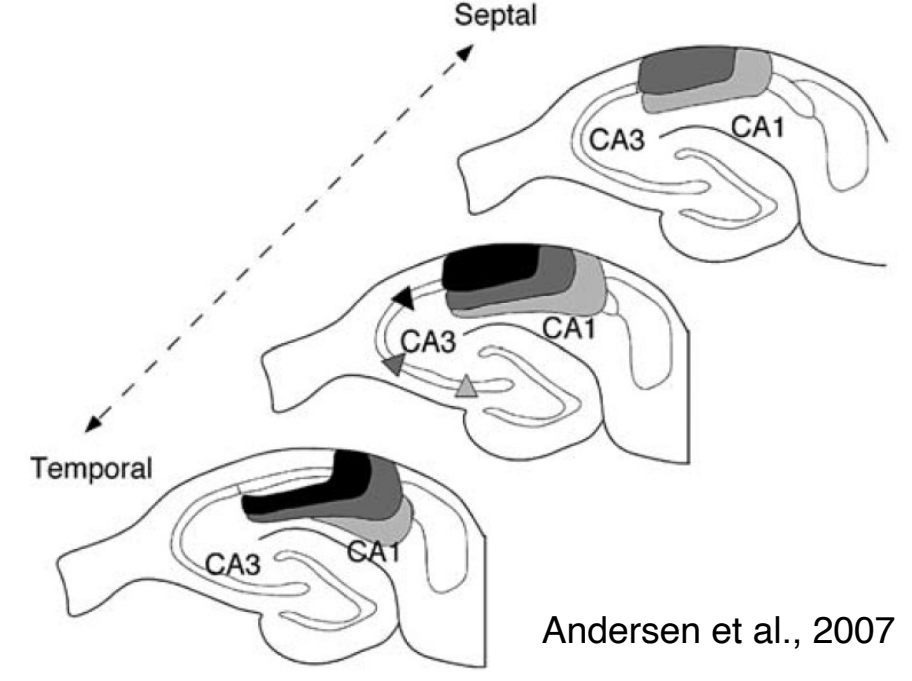






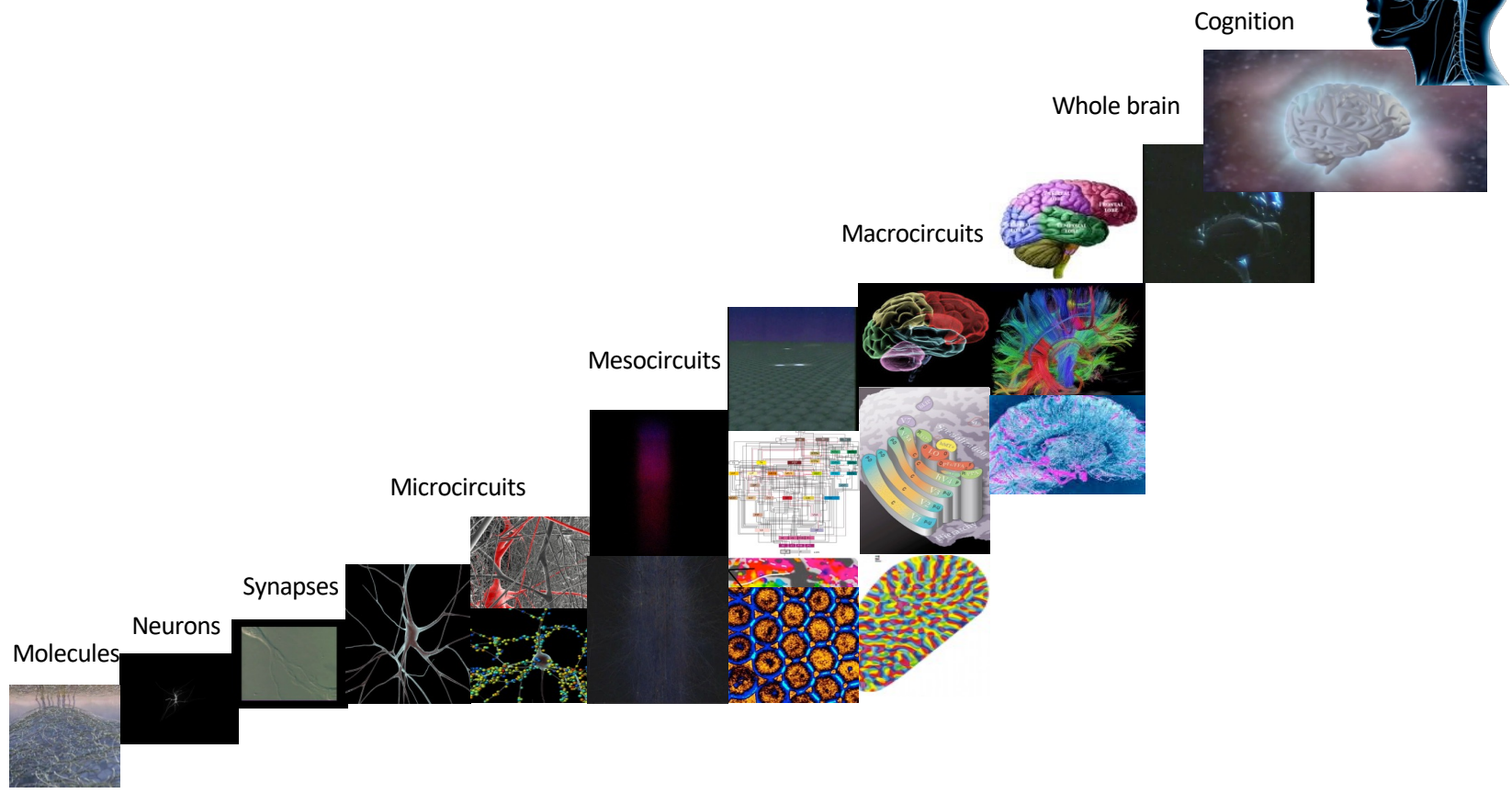
The major organizational features of this projection are as follows: CA3 cells located close to the dentate gyrus (proximal CA3), although projecting both septally and temporally, project more heavily to levels of CA1 located septal to their location. CA3 cells located closer to CA1, in contrast, project more heavily to the levels of CA1 located temporally (Fig. 3-30). At or close to the septotemporal level of the cells of origin, those cells located proximally in CA3 give rise to collaterals that tend to terminate superficially in the stratum radiatum. Conversely, cells located more distally in CA3 give rise to projections that terminate deeper in the stratum radiatum and stratum oriens. At or close to the septotemporal level of origin, CA3 pyramidal cells located near the dentate gyrus tend to project somewhat more heavily to distal portions of CA1 (near the subiculum), whereas CA3 projections arising from cells located distally in CA3 terminate more heavily in portions of CA1 located closer to CA2.

Figure 3–30. Organization of the projections from the CA3 field to the CA1 field of the hippocampus—the Schaffer collaterals. The location of the cells of origin is indicated by small triangles in the middle coronal section. Terminals from these cells are indicated by different shades of gray similar to those in the triangles.





Different scales





Clinical

Experimental techniques

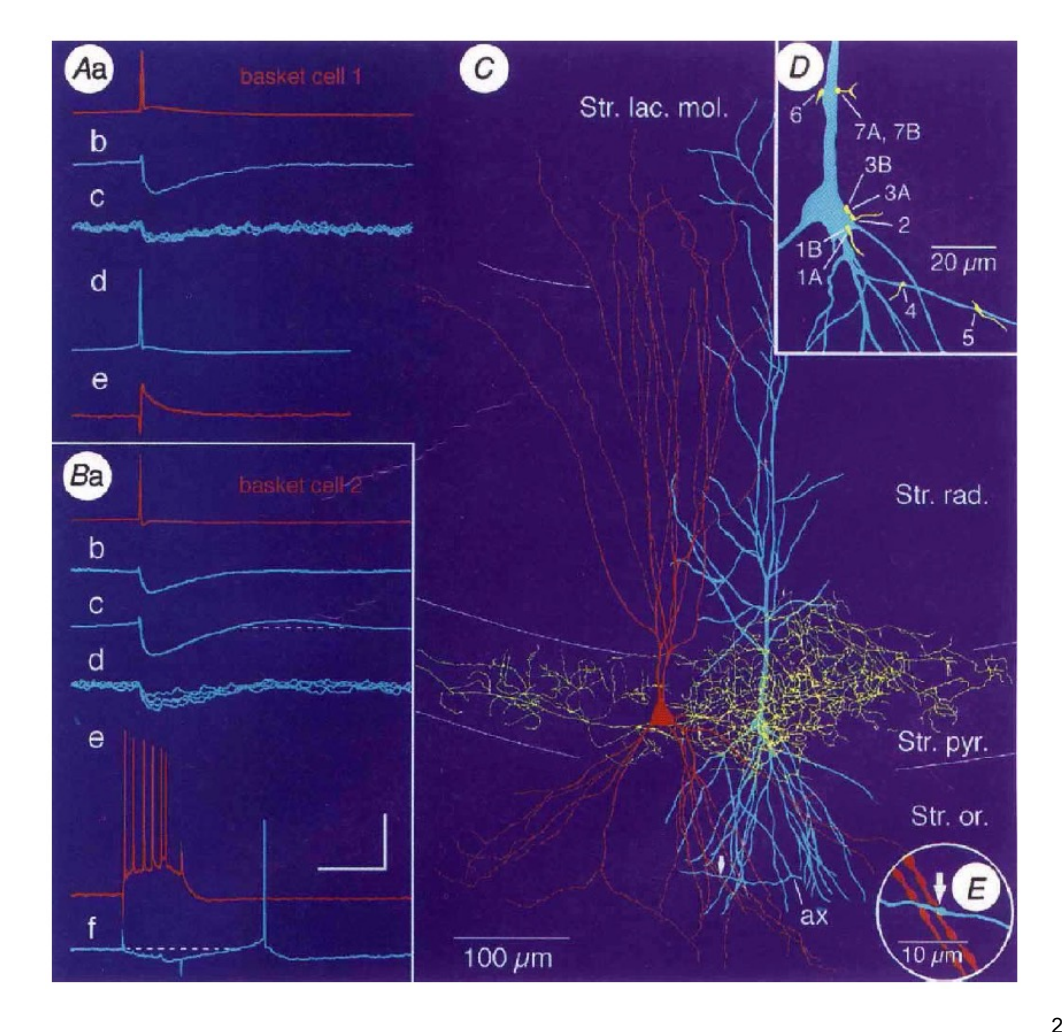
- Light microscopy
- Electron microscopy
- Neuronal tracer
- Transsynaptic labelling
- Pair recording
- Multi-patch clamp
- Tractography



Light microscopy

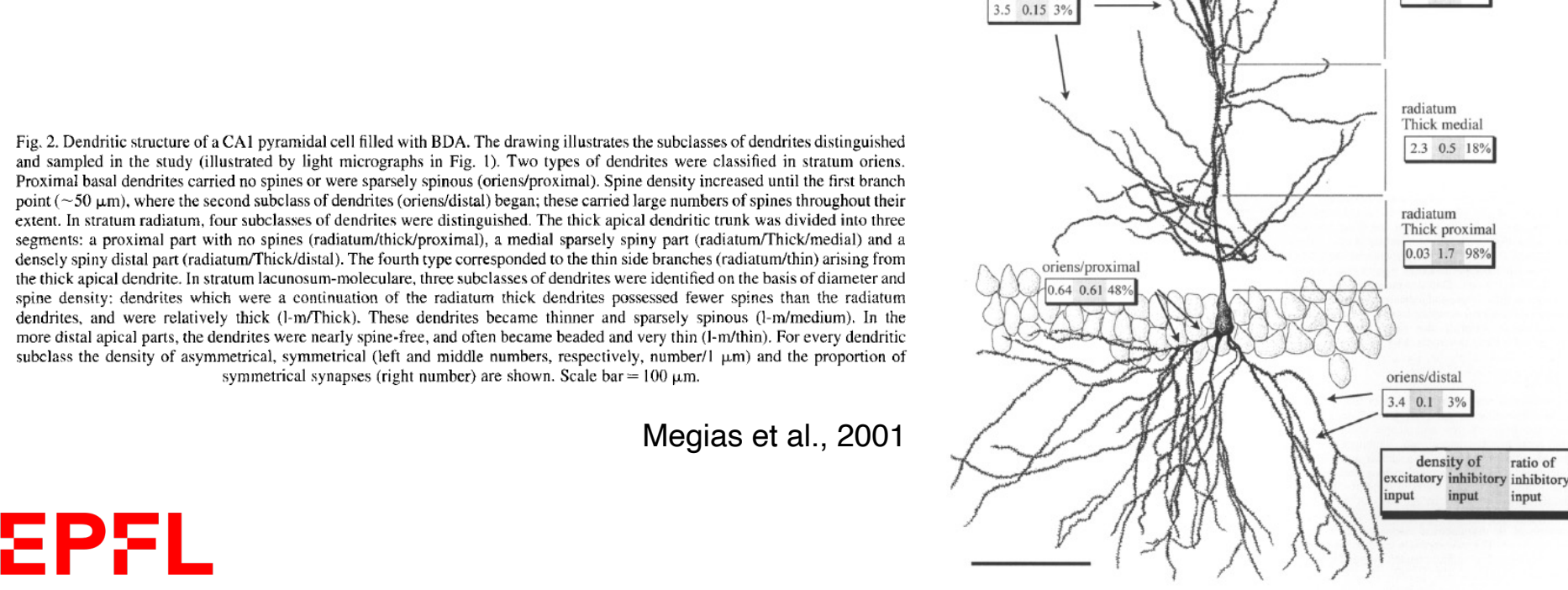
D, Location of 10 synaptic junctions (see Fig. 4 for example) by electron microscopy, received by the postsynaptic pyramidal cell shown in C, giving the postsynaptic effect shown in Ab. Three boutons (numbers 1, 3 and 7) made 2 synaptic junctions each. E, Enlargement of the area labelled by small arrow in C, showing a recurrent collateral of the pyramidal cell axon (ax) which is in contact with a basket cell dendrite. Subsequent electron microscopy revealed that a single synaptic release site (arrow; also shown in Fig. 4c) mediated the recurrent e.p.s.p. shown in Ae. Str. lac. mol., stratum lacunosum moleculare; Str. rad, stratum radiatum; Str. or., stratum oriens. Scale bars in A and B: Aa, d and Ba: 40 mV; Be and f: 20 mV; Ac and Bd: 5 mV; Ab, e and Bb, c: 1 mV; A and Ba-d: 50 ms; Be and f: 100 ms.

Buhl et al., 1994





Light microscopy



1-m/Thick

1.72 0.28 14%

radiatum/thin

1-m/thin 0.4 0.09 179

radiatum Thick distal

6.9 0.15 2%

l-m/medium

0.8 0.12 15%

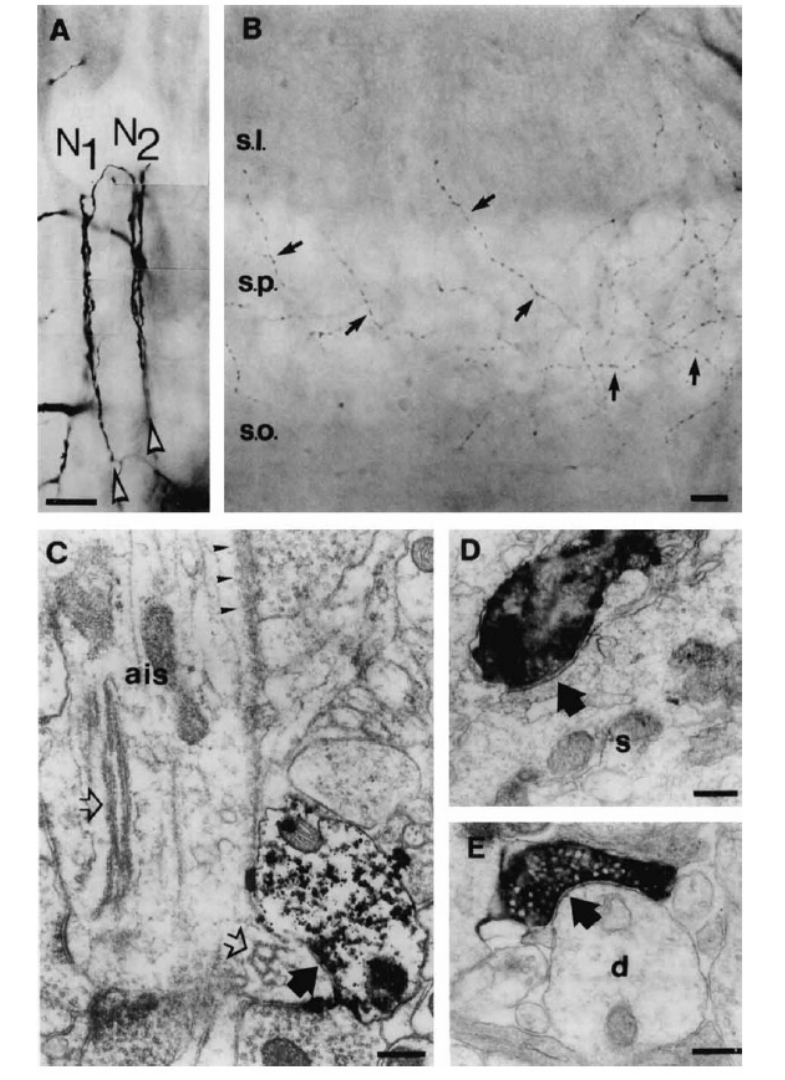


Electron microscopy

FIGURE 3. Light and electron micrographs of axo-axonic (A,C) and basket cell (B,D,E) axon collaterals. A: Axon collaterals (arrowheads) of a Golgi-impregnated axo-axonic cell in the monkey hippocampal CA1 region climb along the axon initial segments of two unstained pyramidal cells (N1 and N2). B: Basket cell collaterals (arrows) also form rows of boutons in strata pyramidale, proximal oriens, and radiatum, but these segments have no preferred orientation, unlike axo-axonic cells, which have numerous radially oriented terminal segments. Basket cell axons pass among the tightly packed pyramidal cell bodies and occasionally follow apical or basal dendrites into strata radiatum or oriens. The layers of the CA3 subfield are indicated. s.o., stratum oriens; s.p., stratum pyramidale; s.l., stratum lucidum. C: Electron micrograph of an axon terminal of a Golgi-impregnated axo-axonic cell from the rat hippocampus, forming a symmetrical synapse (black arrow) on a spinelike appendage of an axon initial segment (ais). Ultrastructural characteristics of axon initial segments include an electron-dense membrane undercoating (arrowheads) and lamellar bodies (open arrows). D,E: Axon terminals of an intracellularly filled basket cell in the guinea pig hippocampal CA3 region form symmetrical synapses (arrows) on a cell body (s in D) and on a dendritic shaft (d in E). Data from Gulyás et al. (1993a) and Somogyi et al. (1983a, 1985a). Scale bars = 10 µm for A,B, 0.2 μm for C-E.

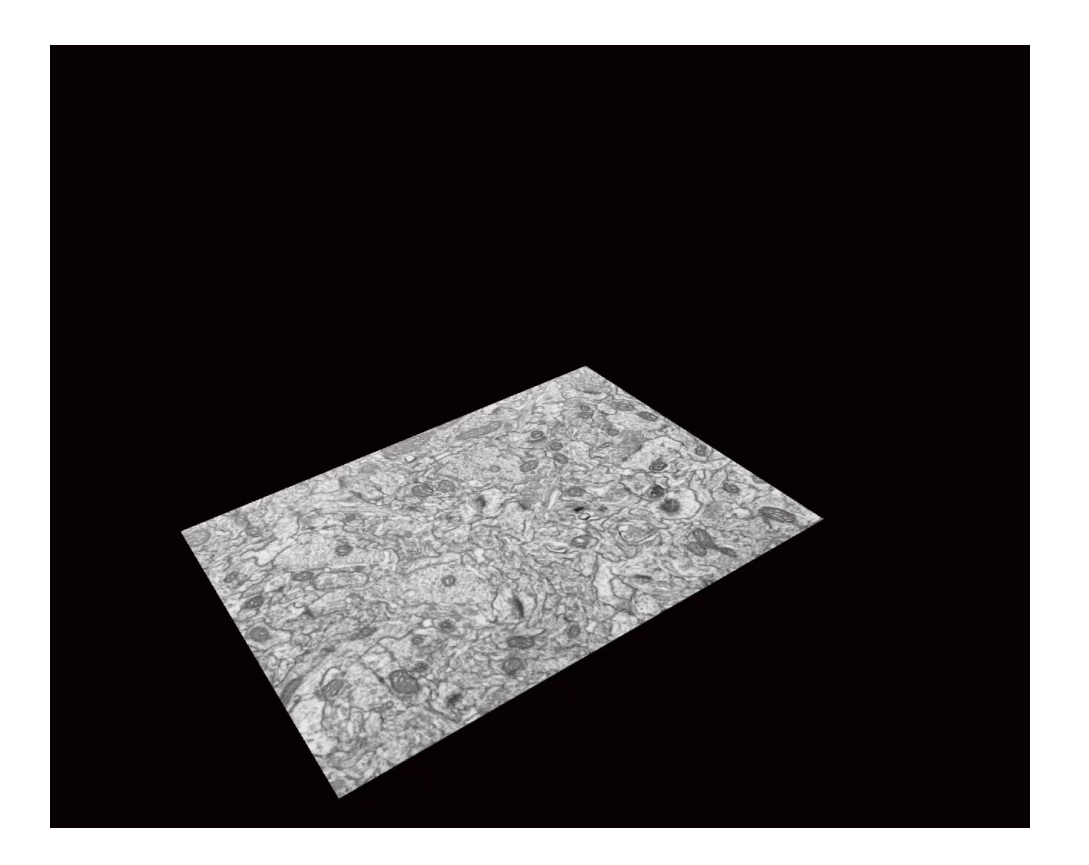






Electron microscopy

- L3 of young rat SSCx
- fully reconstruction of 1695
 synaptic junctions
- 3D organization is nearly random, only constrained by the fact that synapses cannot overlap in space



Merchán-Pérez et al., 2014



Neuronal tracer

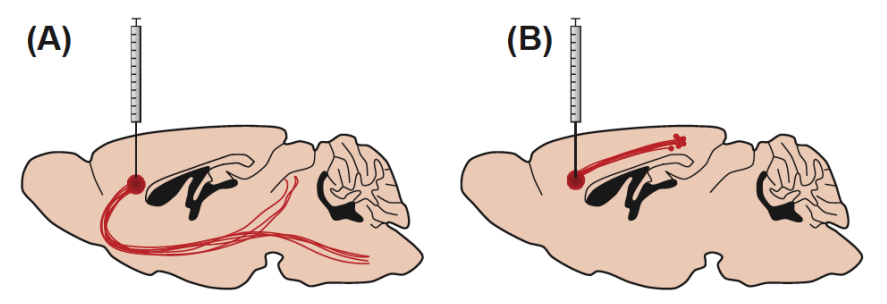


FIGURE 6.9 Anterograde and retrograde tracers. (A) Anterograde tracers show efferent projections, revealing regions that *receive* projections from cells in the labeled area. (B) Retrograde tracers show afferent projections, indicating regions that *project to* the labeled area.

Carter and Shieh, 2015

TABLE 6.4 Classical Anterograde and Retrograde Tracers		
Direction	Comments	
Retrograde	Produces brown precipitate after reaction with hydrogen peroxide and DAB (diaminobenzidine)	
Retrograde	Available in many different colors; nontoxic	
Retrograde	Widely used, rapid labeling	
Retrograde	Produces yellow fluorescence	
Retrograde	Stable, rapid labeling; produces blue fluorescence	
Retrograde	May also be anterograde	
Anterograde and retrograde	Lipophilic dye crystals	
Anterograde and retrograde	Widely used; direction of transport depends on molecular weight and pH; can be visualized by EM	
Anterograde	Plant lectin; can be visualized by EM	
	Direction Retrograde Retrograde Retrograde Retrograde Retrograde Retrograde Anterograde and retrograde Anterograde and retrograde	



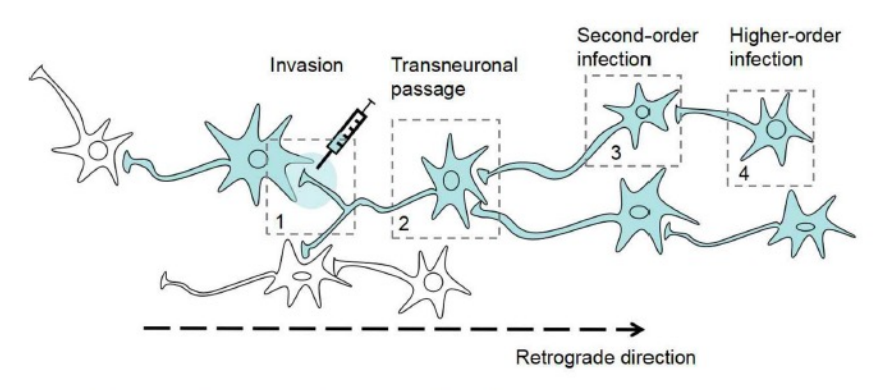
Transsynaptic labelling

TABLE 6.4 Classical Anterograde and Retrograde Tracers			
Tritiated amino acids (³ H-proline, ³ H-leucine)	Transsynaptic (anterograde)	Detected using autoradiography	
Wheat germ agglutinin (WGA)	Transsynaptic	Plant lectin; anterograde and retrograde transport possible; often conjugated to HRP for detection; transgene encoding WGA can be used to label genetically defined neural circuits	
Tetanus toxin, fragment C (TTC)	Transsynaptic (retrograde)	Transgene encoding TTC can be used to label genetically defined neural circuits; nontoxic fragment	
Pseudorabies virus (PRV)	Transsynaptic	Does not infect primates, including humans; bartha strain most commonly used for tracing studies; less virulent, only retrograde transport	
Herpes simplex virus (HSV)	Transsynaptic	Broad host range, including humans	

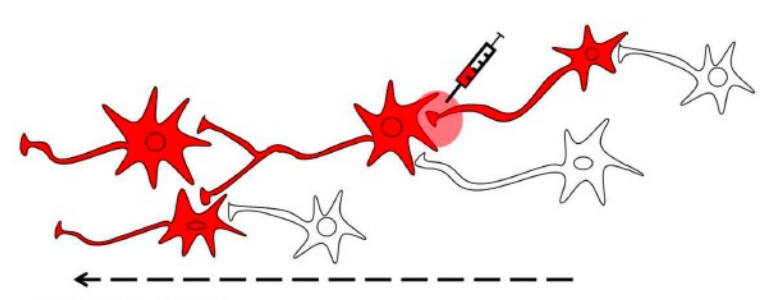
Carter and Shieh, 2015



A Retrograde tracing using transsynaptic viral tracer



B Anterograde tracing using transsynaptic viral tracer



Anterograde direction

Fig. 1 Schematic of tracing using trans-synaptic viral tracers. A By injecting a retrograde viral tracer into region 1, the virus first infects the axons/dendrites/somata of first-order neurons in the injection site. Then, by trans-synaptic transmission in region 2, it spreads further to the synaptically-connected presynaptic second-order neurons in

region 3. In this way, viral tracer can infect the presynaptic neurons connected with specific neurons and enable the tracing of chains of connected neurons. B Trans-neuronal anterograde tracing is the spread from presynaptic neurons to postsynaptic neurons by transsynaptic transmission.

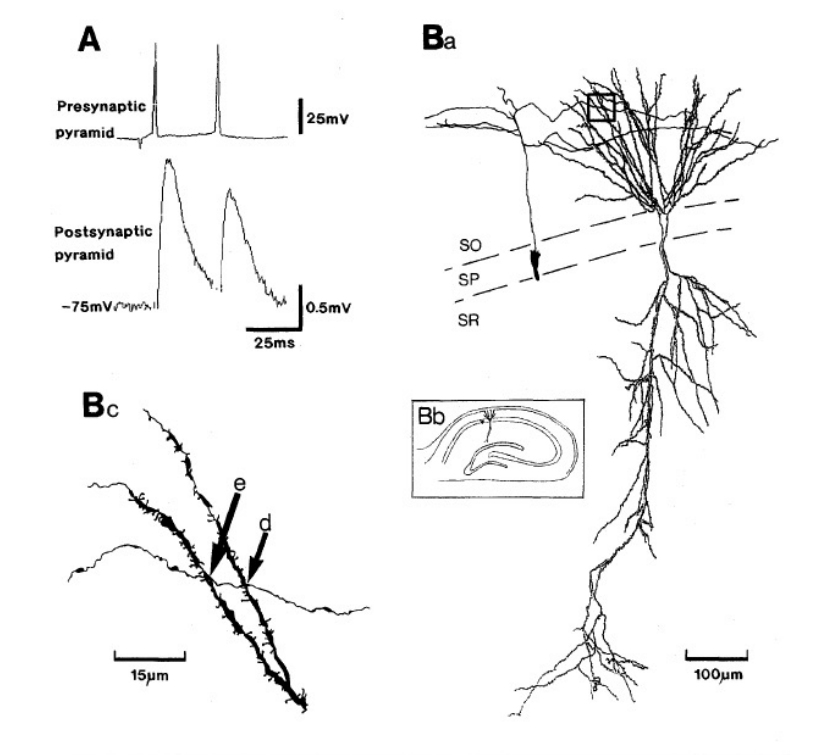
Li et al., 2019

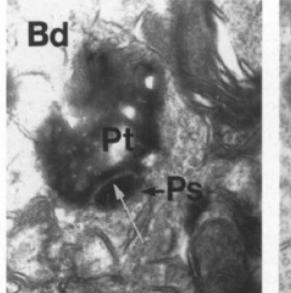
Pair recording

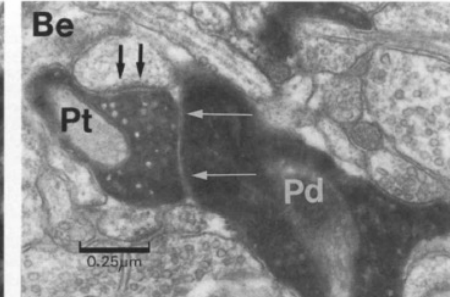
In 11 experiments, involving 56 transverse hippocampal slices, 989 pairs of CA1 pyramidal neurons were tested for synaptic connections.

[...] Nine of the 989 paired recordings yielded monosynaptic EPSPs. In six of these, both cells were sufficiently stable for some of the characteristics of the connection to be studied.

Distance x axis (mean \pm SD, n= 9) 62.8 \pm 72 mm [range 2-201]. Distance y axis (mean \pm SD, n=9) 17.3 \pm 19.2 mm [range 3-58]. [personal communication]

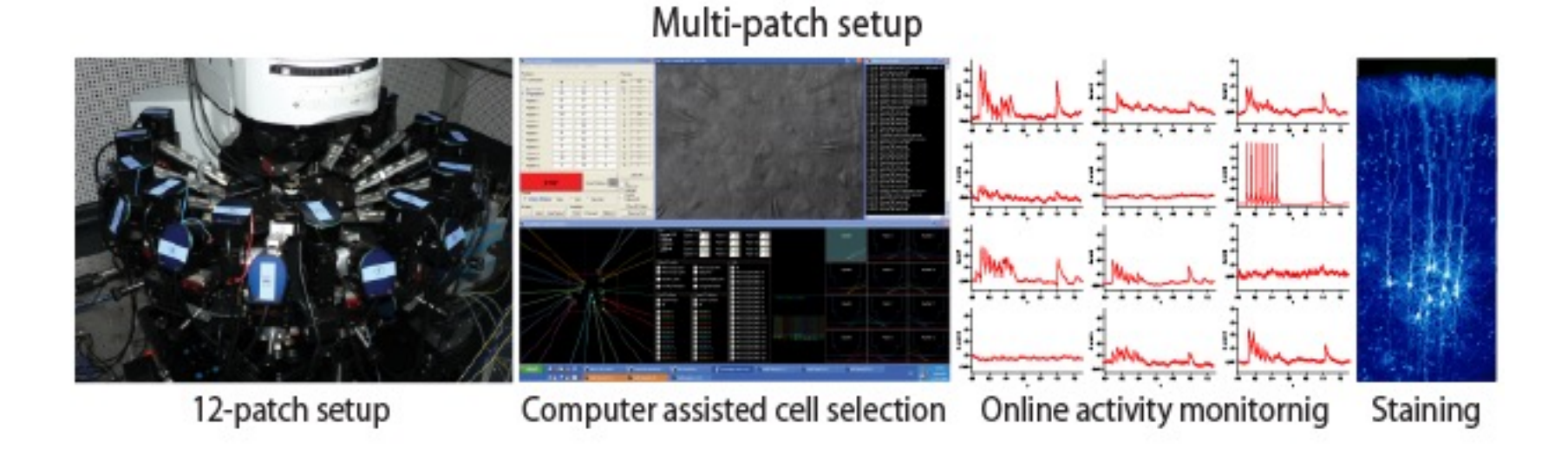








Multi-patch clamp





Tractography

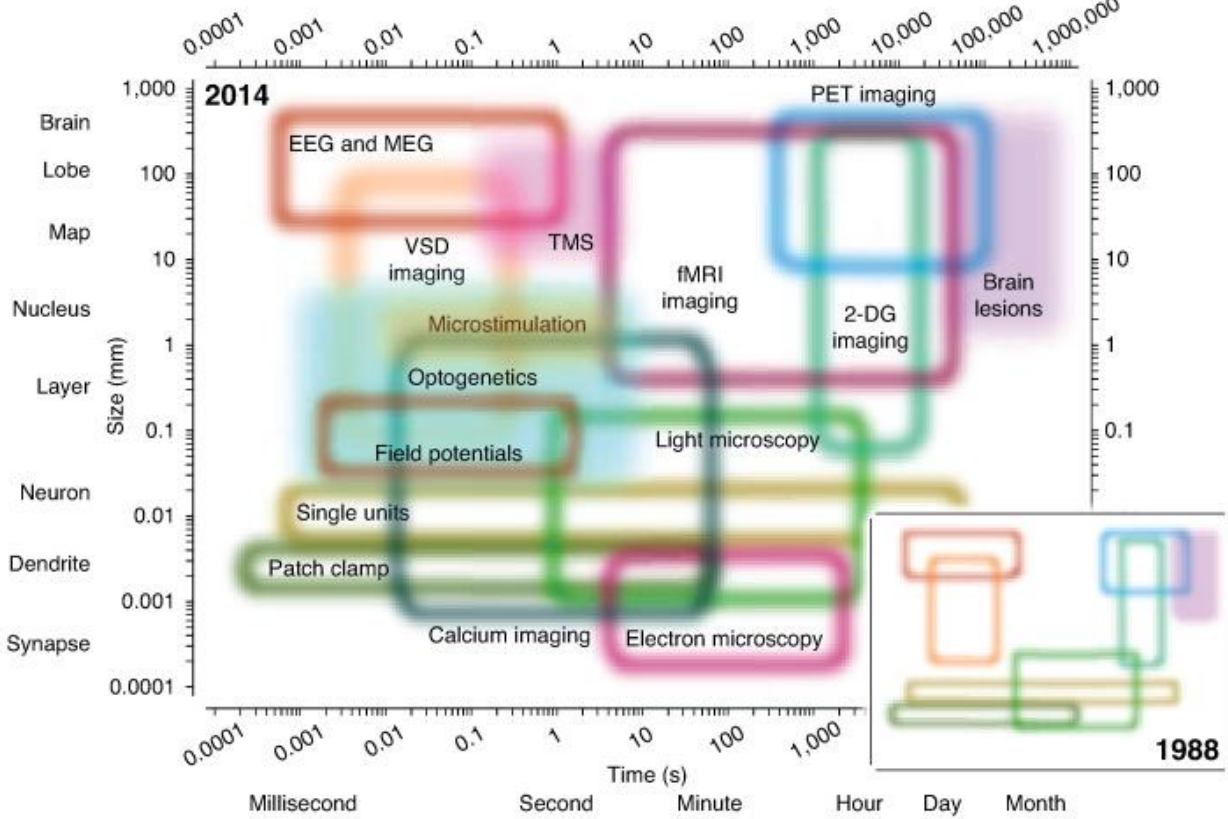
- Diffusion MRI is an application of MRI that is used to examine the structure of axon fiber tracts in the brain
- Water molecules tend to diffuse most rapidly along parallel bundles of fibers with coherent orientations
- There are various kinds of diffusion
 MRI methods, the most commonly used called diffusion tensor imaging (DTI)



Whole brain fiber tractography using diffusion tensor imaging (www.ExploreDTI.com)



Experimental techniques





Sejnowski et al 2014

Summary 1

- Faithful reconstruction of the set of connections of a brain region (connectome) is a multi-scale problem
- Our tools often investigate the connectome within a certain range of scale
- Merging the scales is still an open issue
- Connectome is a complex network that diverges significantly from random network
- Surprisingly, it shares many features with other complex networks (e.g. social, telecommunication)
- Network science studies those complex networks



Lecture Overview

- Scope
- Approaches
- Applications



Approaches

- No axon, no space approaches
- No axon, space approaches
- Axon, space approaches

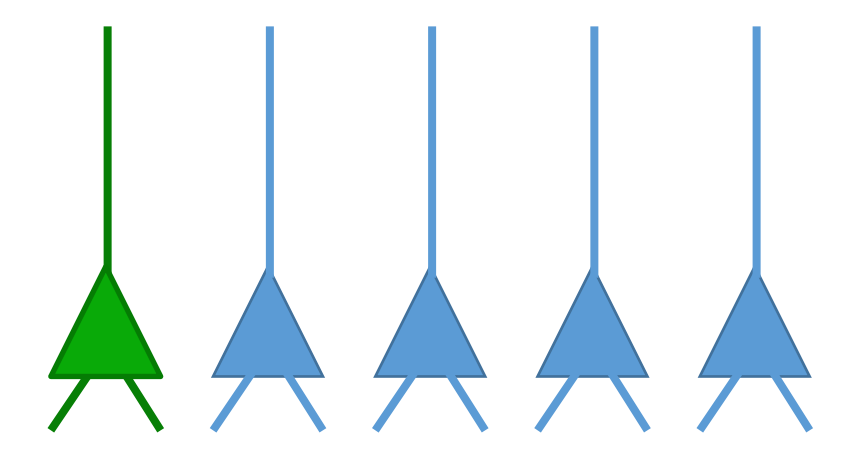


- The axon and the space are not necessary to derive the connectome
- This approach is normally used to connect point neurons
- The simplest approach is random connectivity between cells, where we still
 have to define the 'amount' of connectivity by specifying the target number
 of connection or mean connection probability
- Additional rules can be used to make the connectome more and more realistic



- Cells are placed in a space respecting some constrains about cell density or average inter-somatic distances
- Connections are first of all constrained by distance-dependent connection probability. We have to assume the distribution of the axon, and we have to assume that the axon density is proportional to the connection probability
- We have also to bind the number of connections or synapses by introducing other constrains such as number of synapses per connection, divergence or convergence
- This approach is necessary when we lack of axon reconstructions

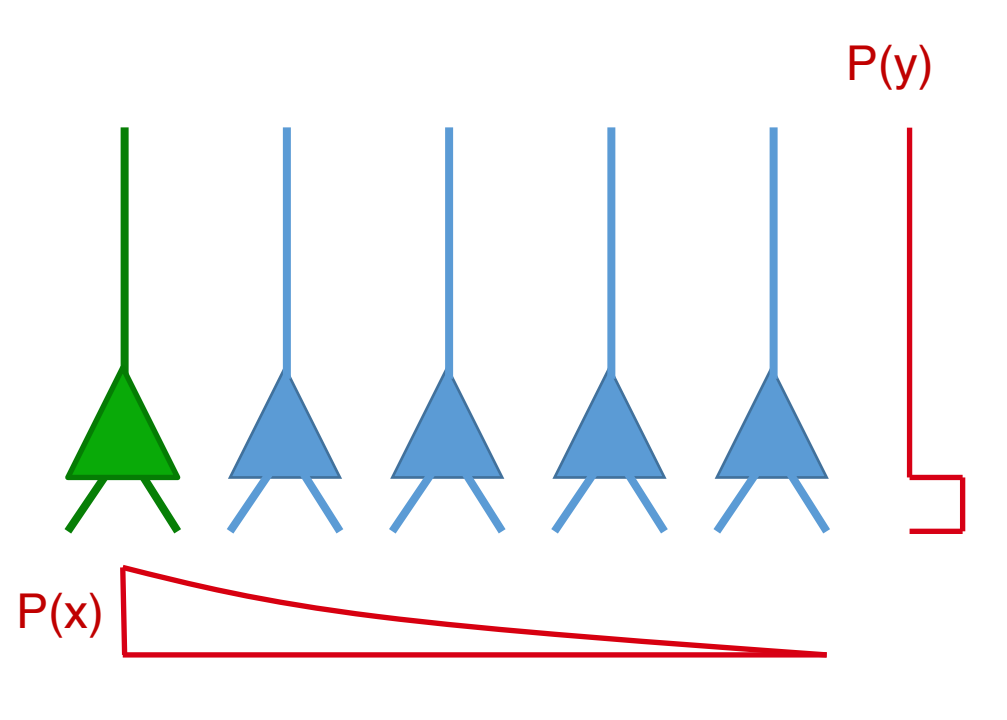




divergence = 2

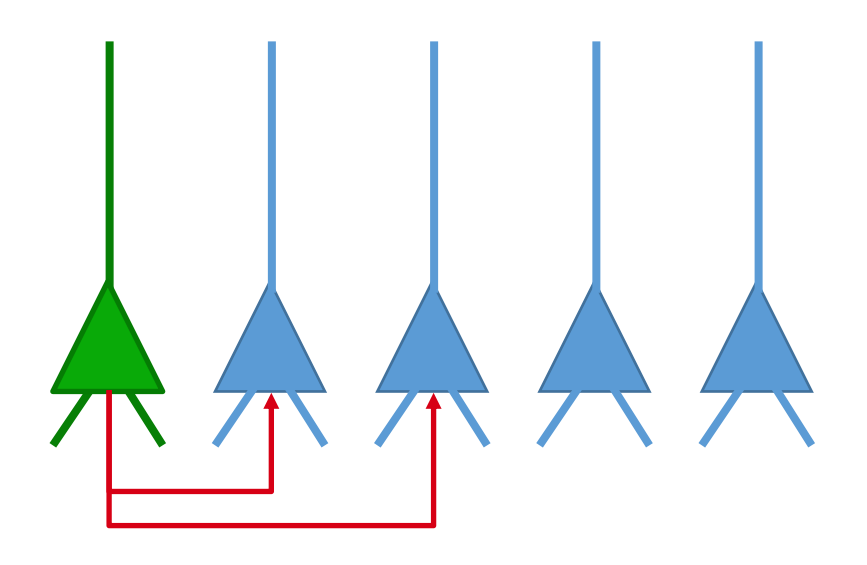
Define the divergence (distribution)





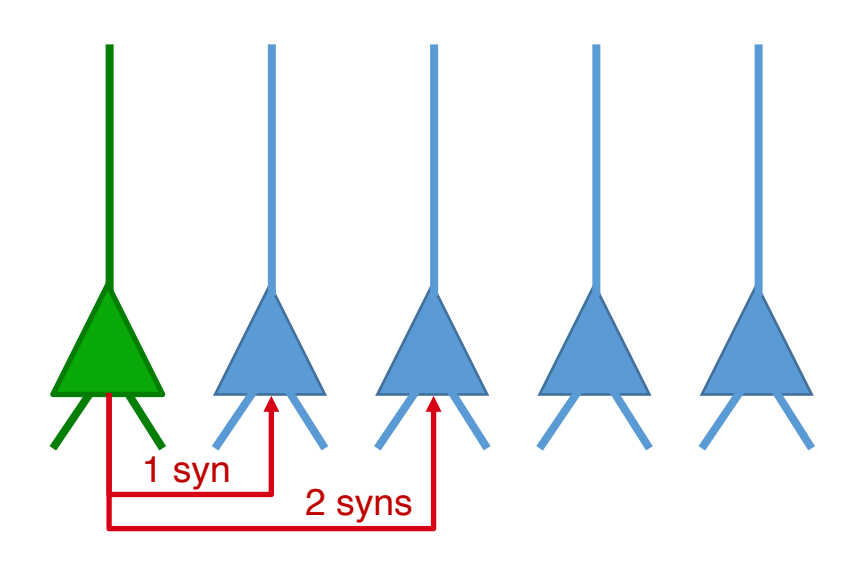
- Define the divergence (distribution)
- Use connection probability to find neurons to connect





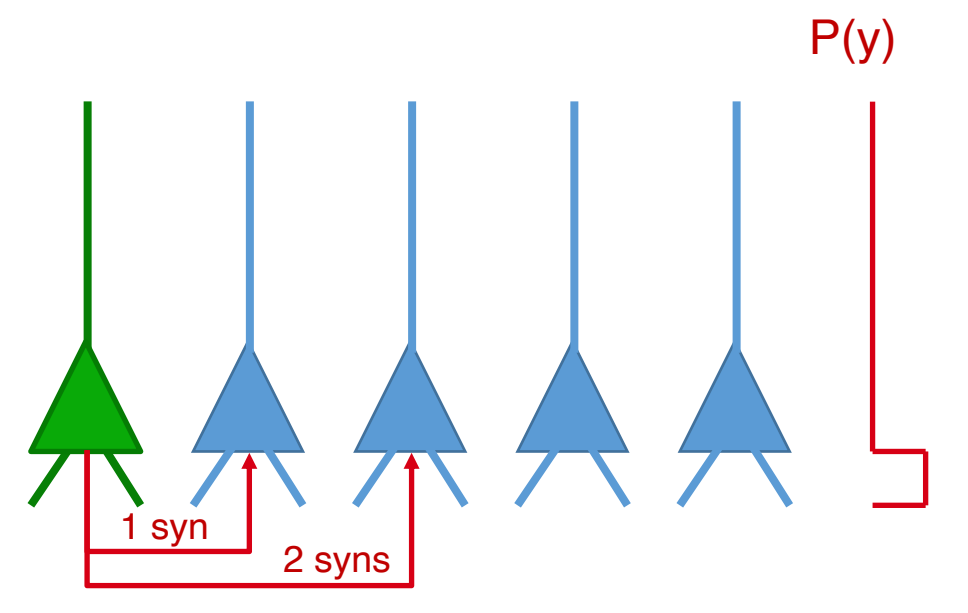
- Define the divergence (distribution)
- Use connection probability to find neurons to connect
- Define number of synapses per connection (distribution)





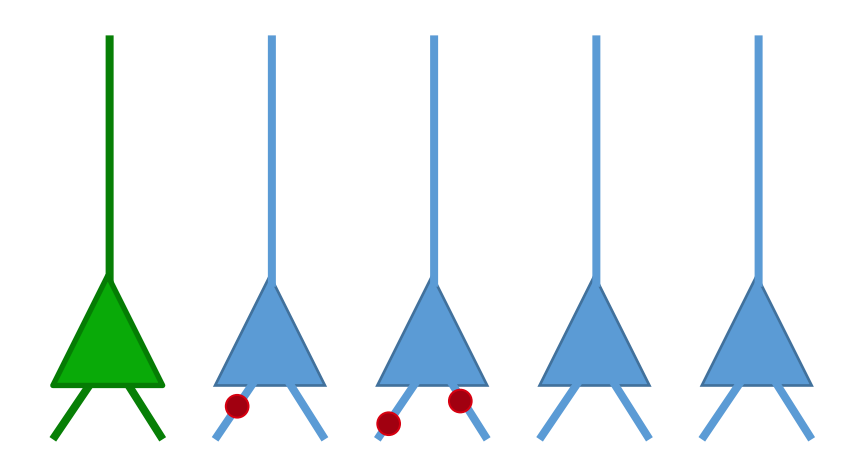
- Define the divergence (distribution)
- Use connection probability to find neurons to connect
- Define number of synapses per connection (distribution)





- Define the divergence (distribution)
- Use connection probability to find neurons to connect
- Define number of synapses per connection (distribution)
- Select n random segment to place n synapses



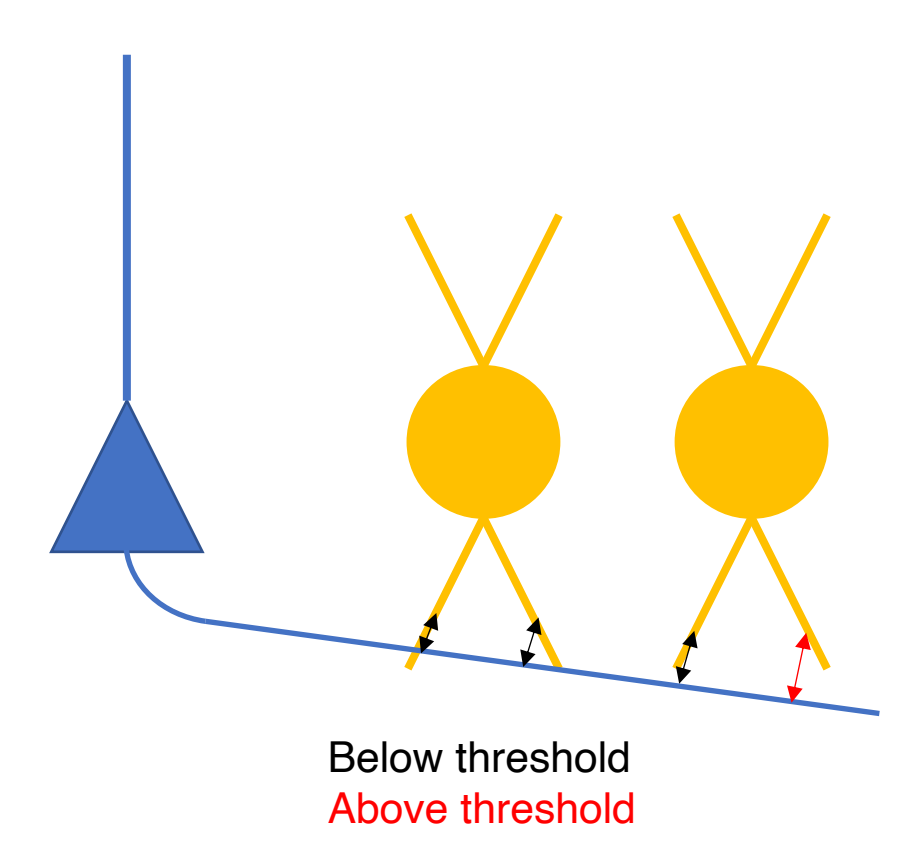


- Define the divergence (distribution)
- Use connection probability to find neurons to connect
- Define number of synapses per connection (distribution)
- Select n random segment to place n synapses
- Place synapses

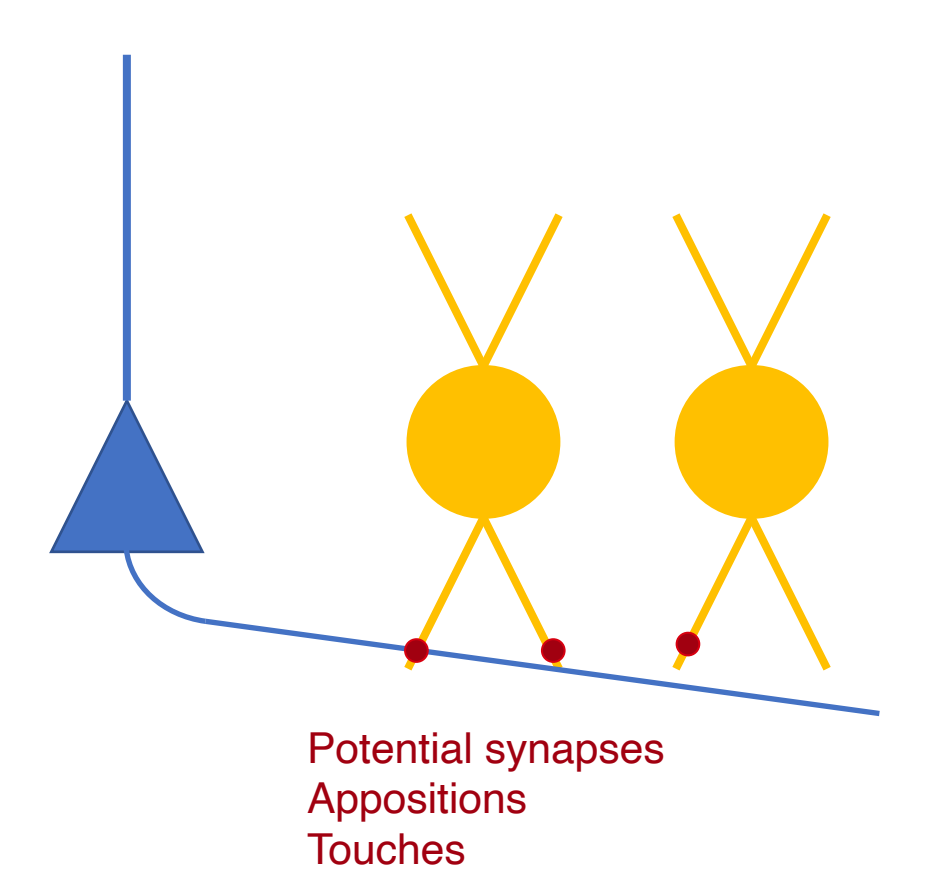


- Proximity between axon and target cells is used to find <u>potential synapses</u> or <u>appositions</u>
- We have to define a threshold for the distances
- This approach often gives more synapses than expected
- Exceeding synapses are discarded with a process called <u>pruning</u>

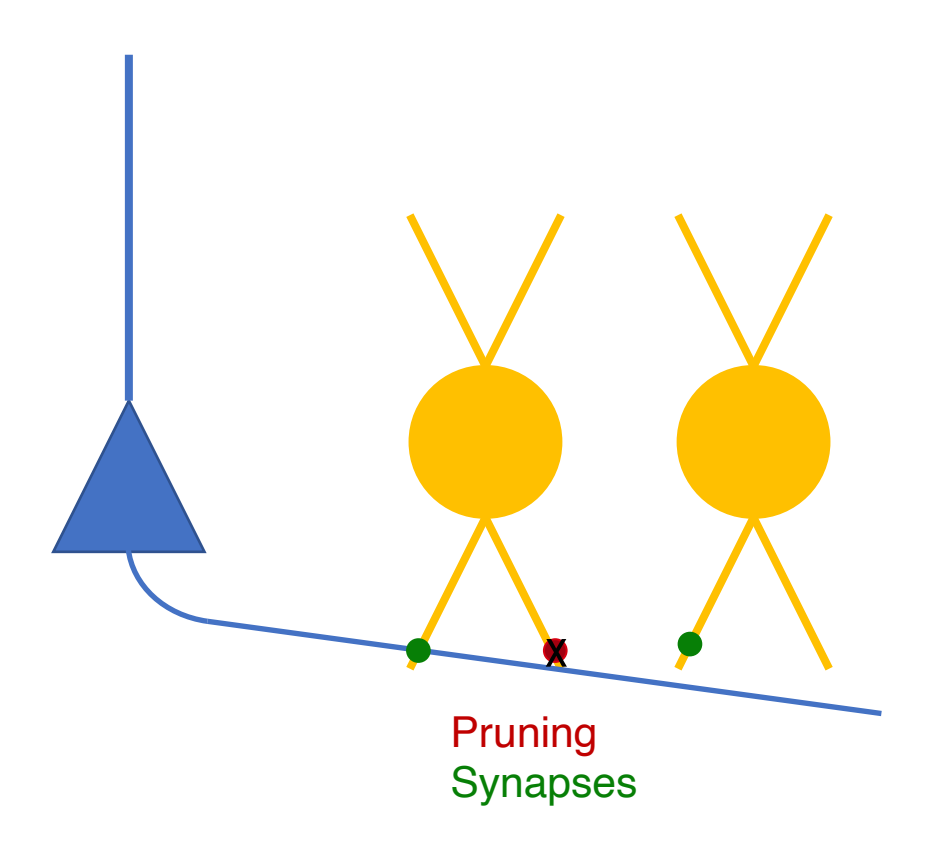






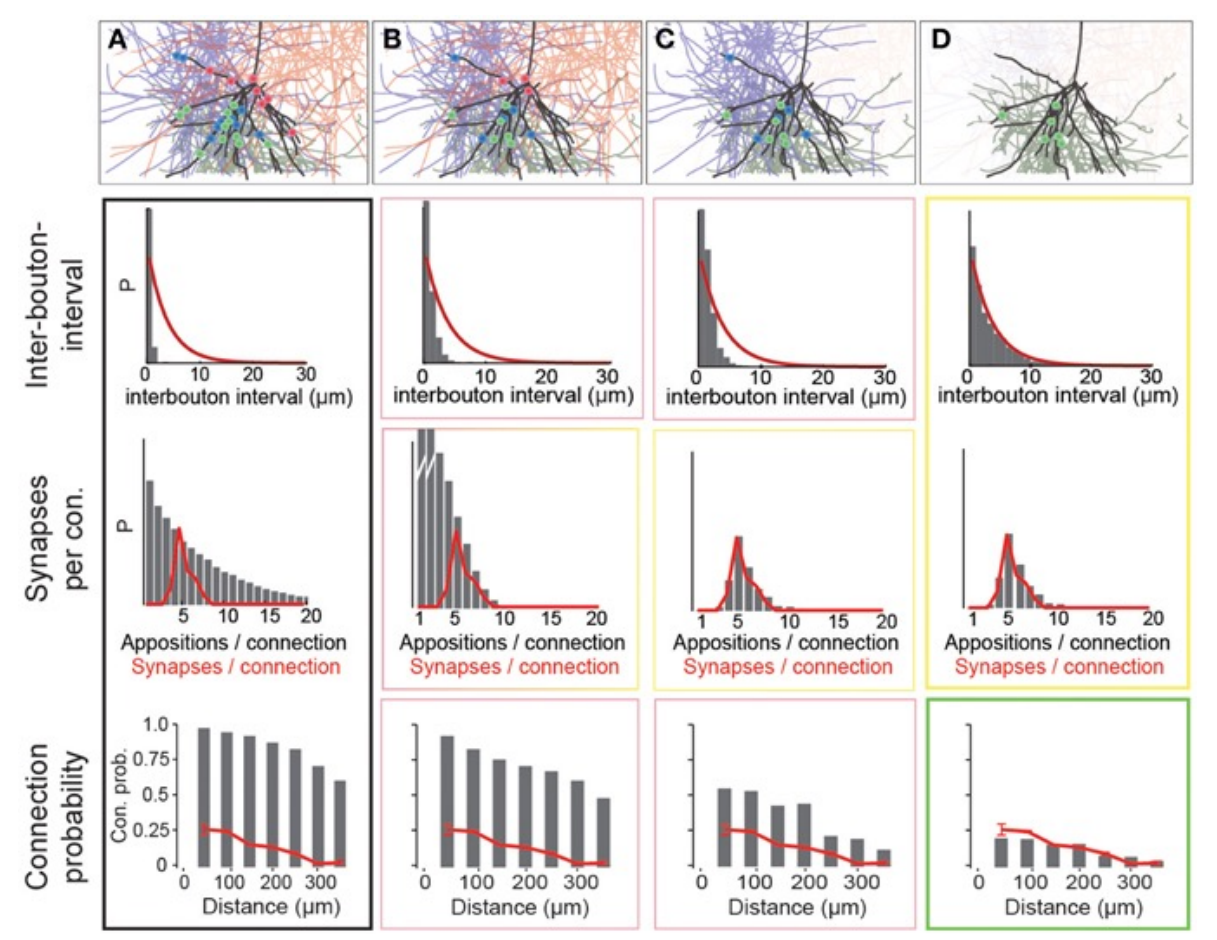








Reimann et al., 2015





Summary 2

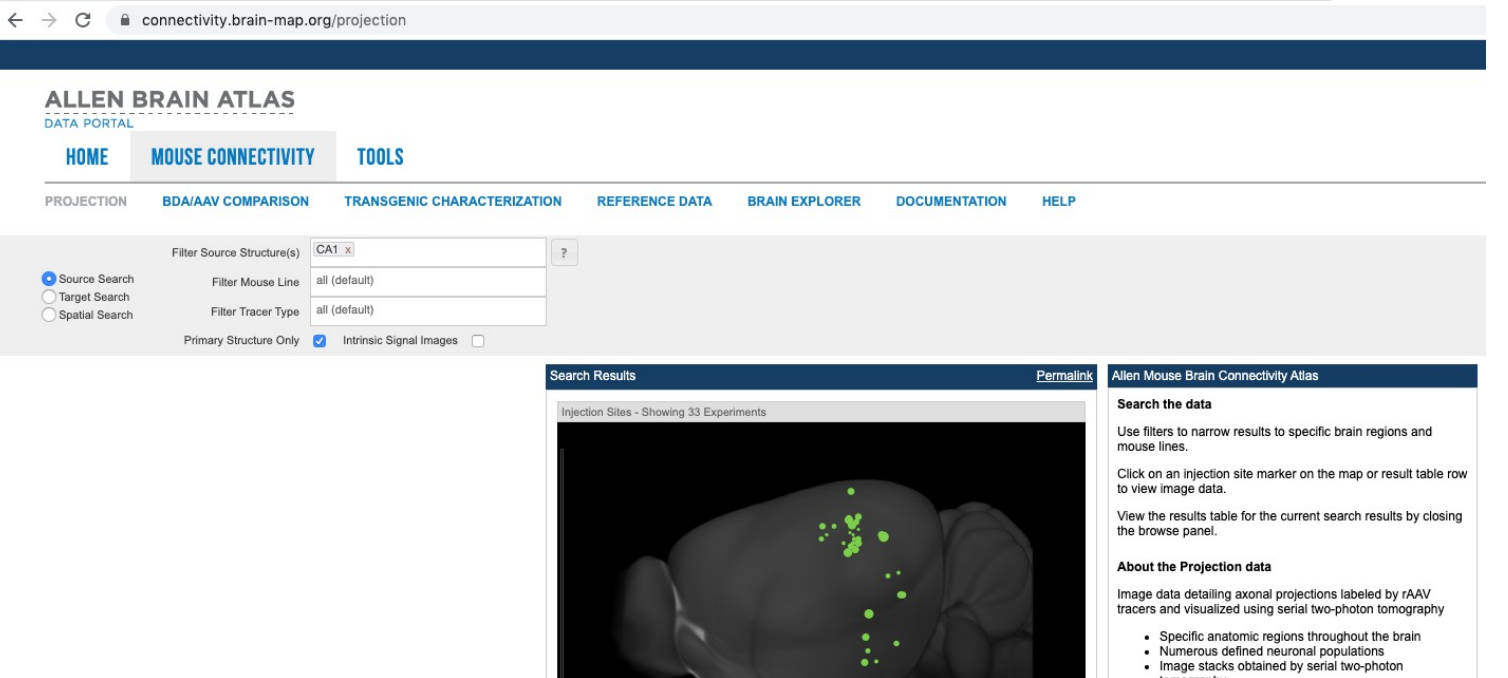
- There are a multitude of approaches but they can categorized in 3 groups depending if we constrain the space or not, and if we have axon or not
- In all approaches we can include more and more constrains to match known data
- Anyway, this with a cost of having an algorithm less predictive, something important when the data are sparse and we have more unknowns that knowns

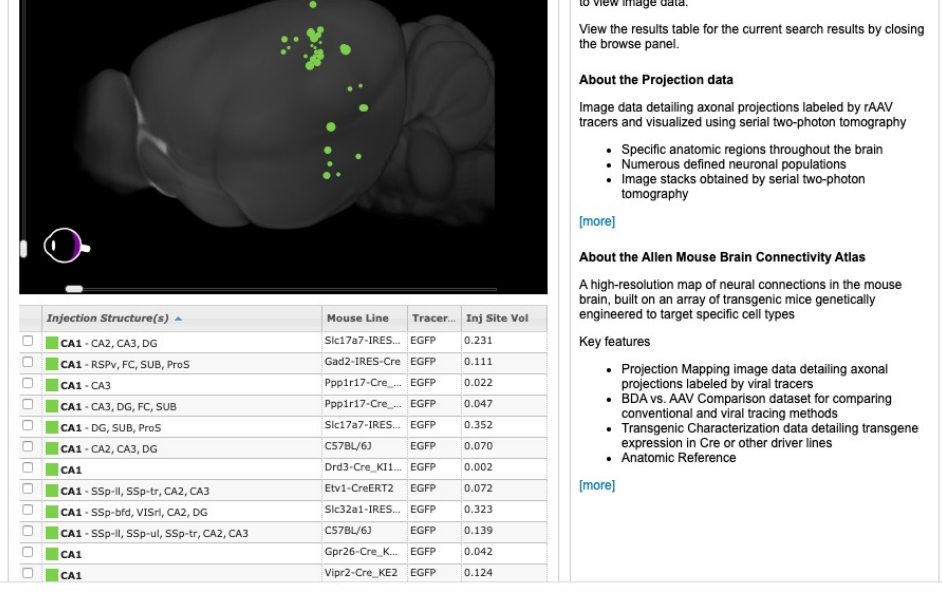


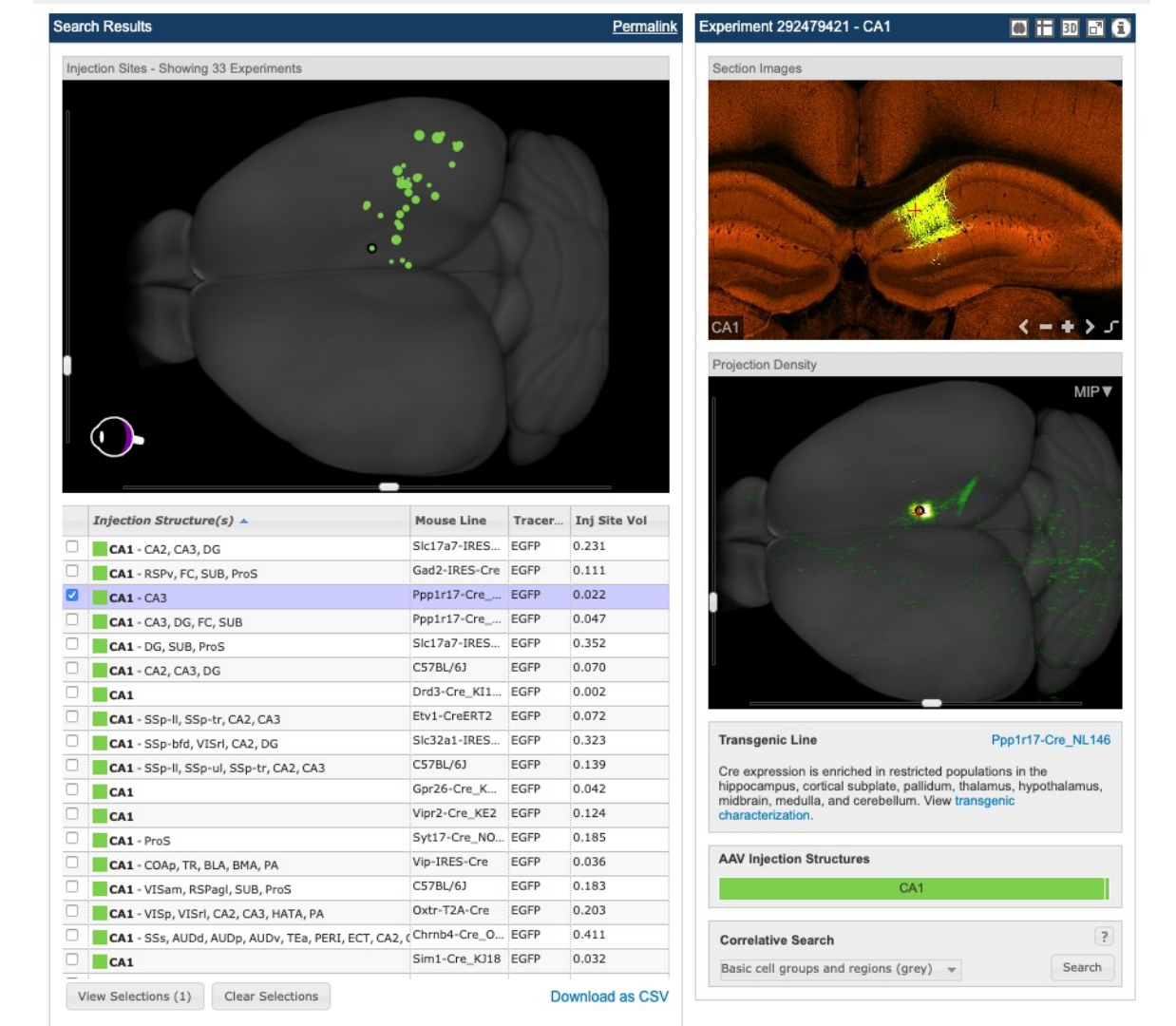
Lecture Overview

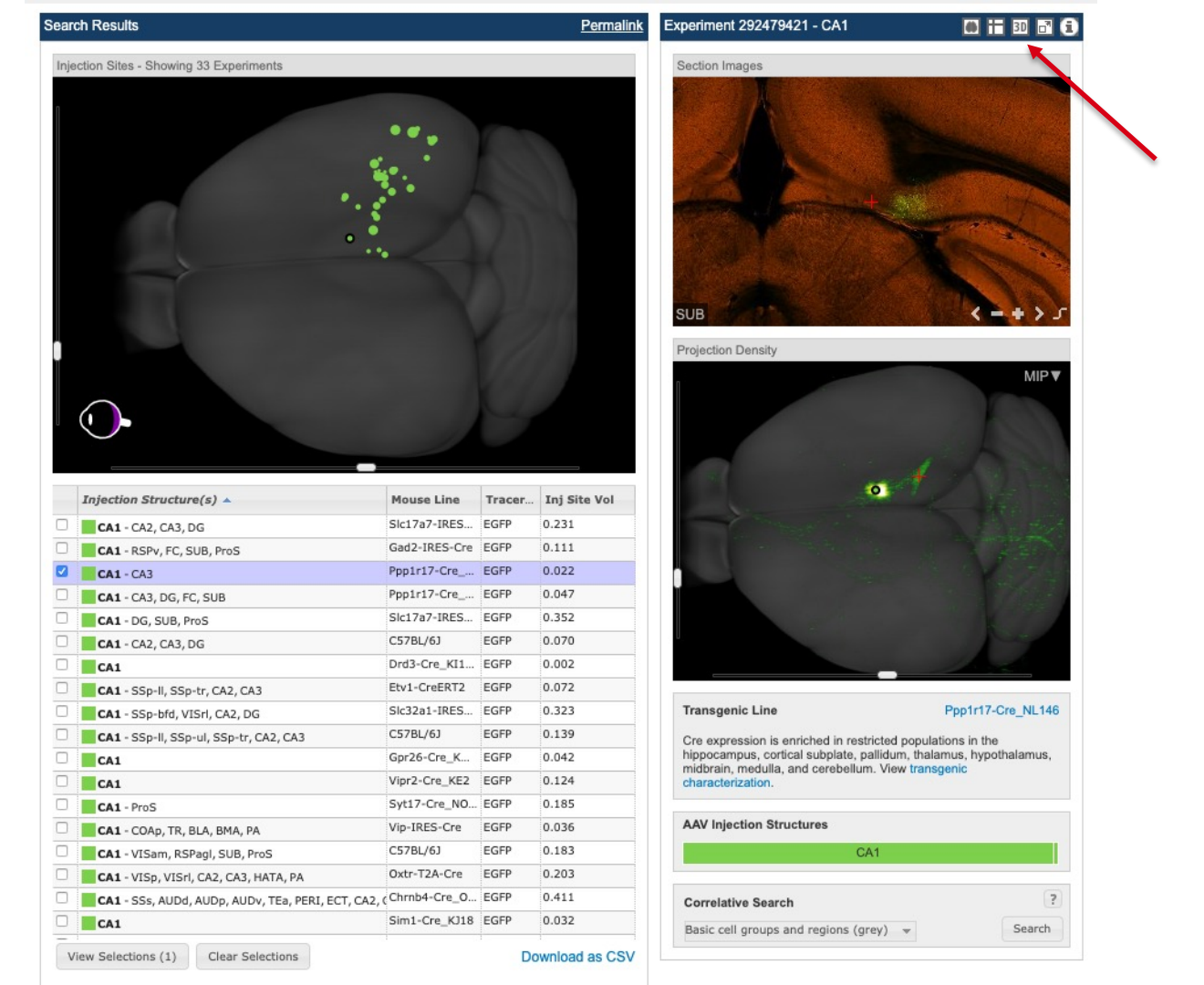
- Scope
- Approaches
- Applications

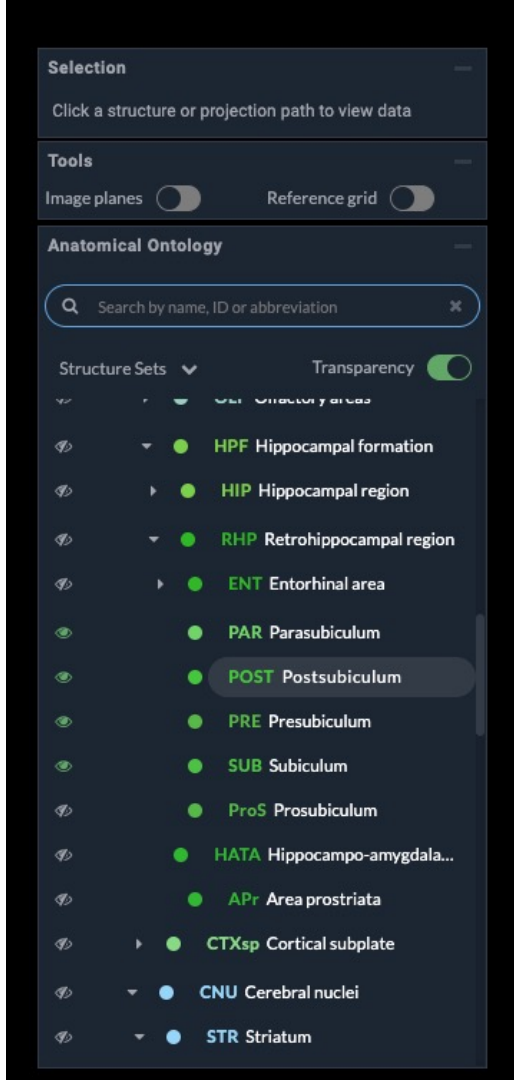


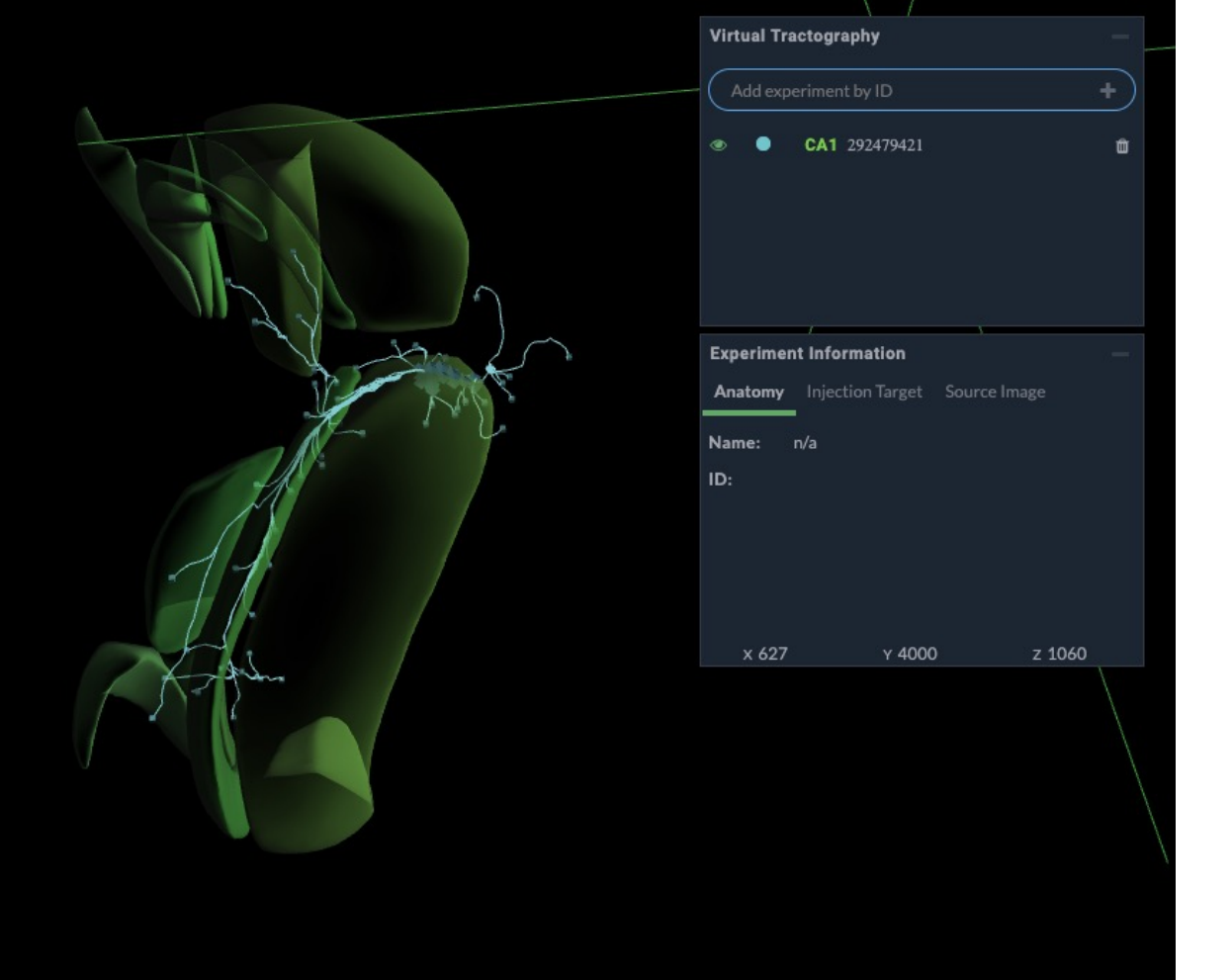








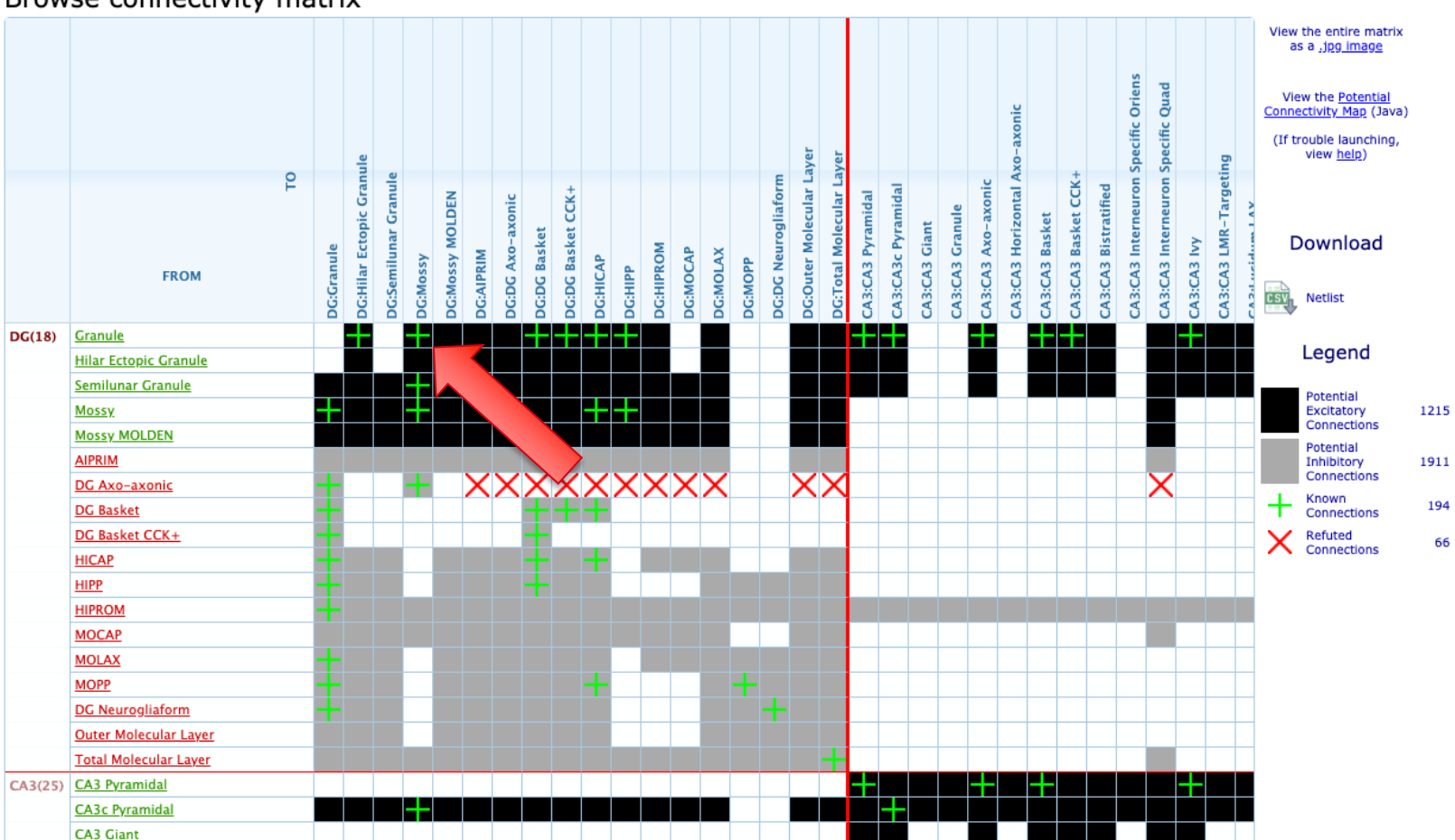






Browse Search Tools Help







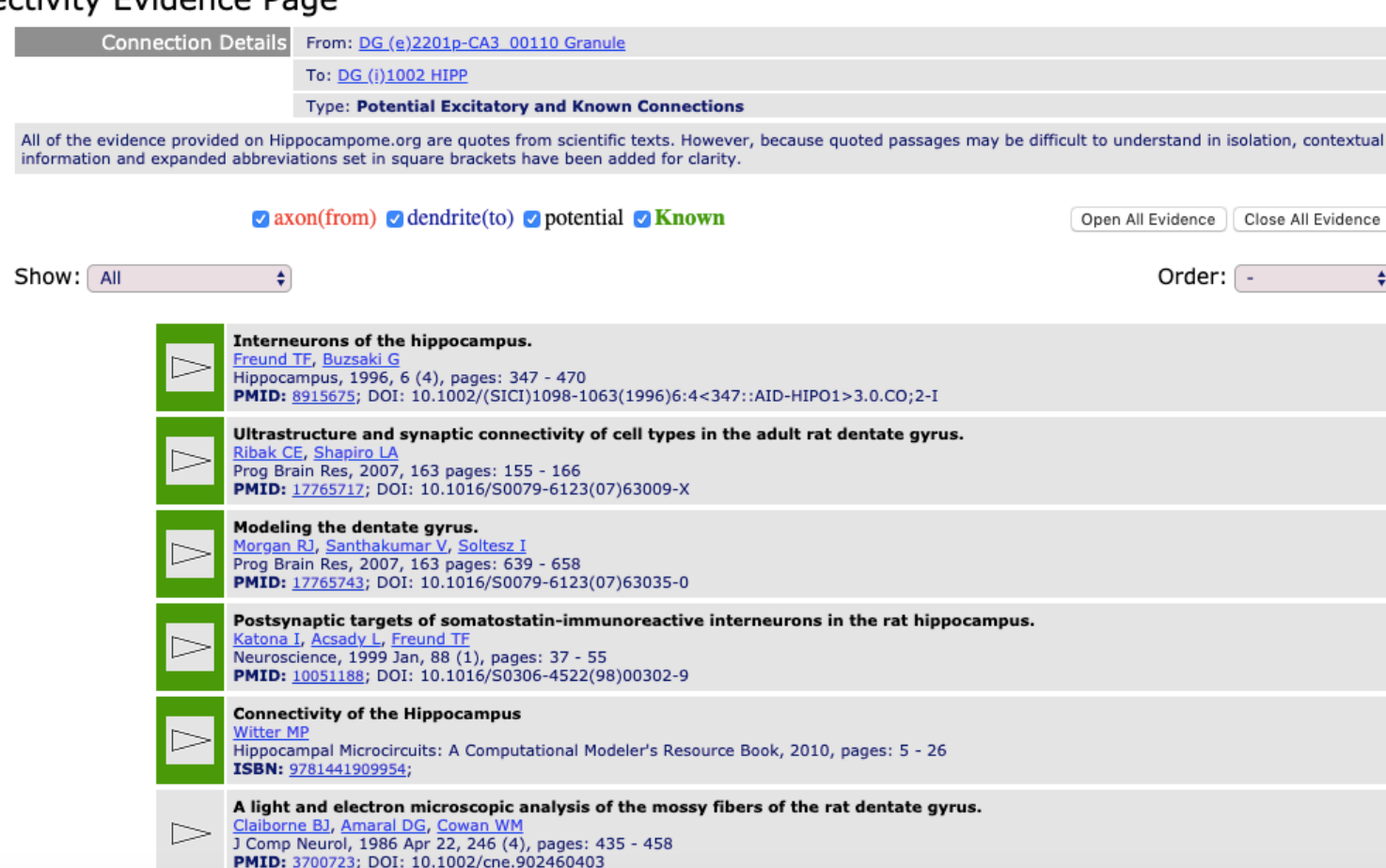








Connectivity Evidence Page

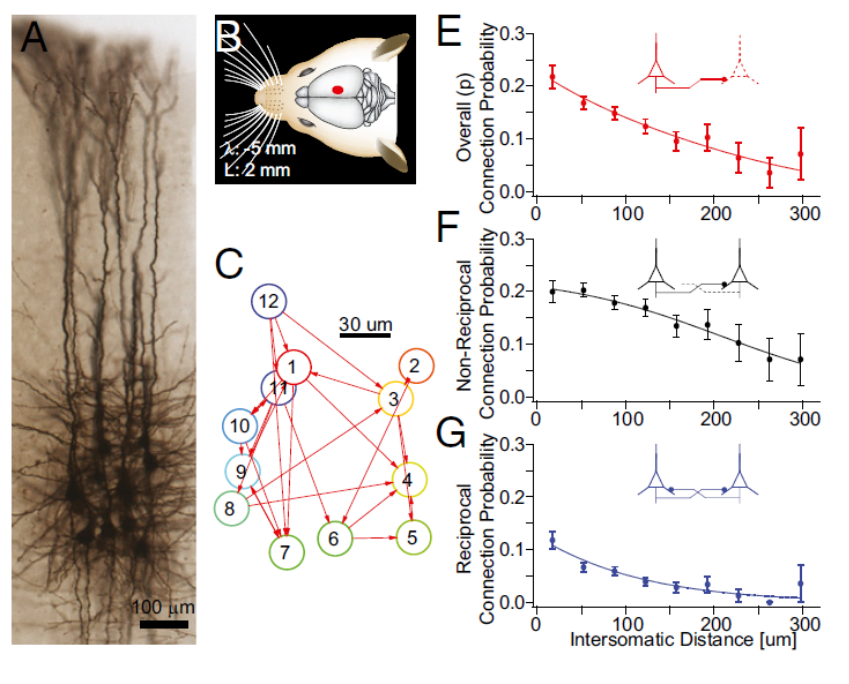


A synaptic organizing principle for cortical neuronal groups

Rodrigo Perin, Thomas K. Berger¹, and Henry Markram²

Blue Brain Project, Ecole Polytechnique Fédérale de Lausanne (EPFL), CH-1015 Lausanne, Switzerland





We recorded simultaneously from up to 12 thick-tufted layer 5 pyramidal neurons in somatosensory cortical slices (300 µm thick) from Wistar rats (postnatal days 14-16).

These data also confirm previous reports that bidirectional connections are more than two times as frequent than predicted by chance (Fig. 1G).

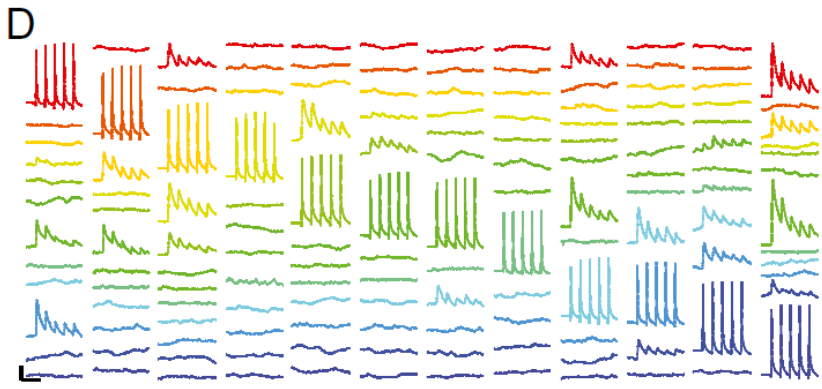
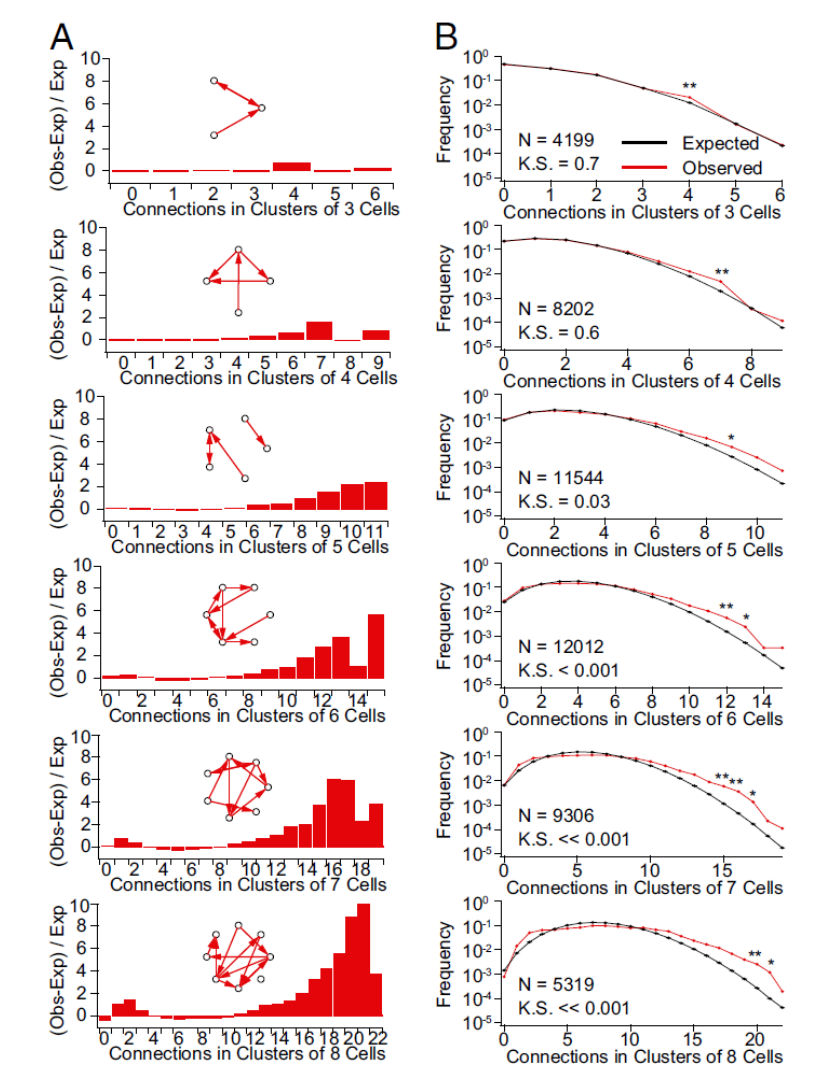
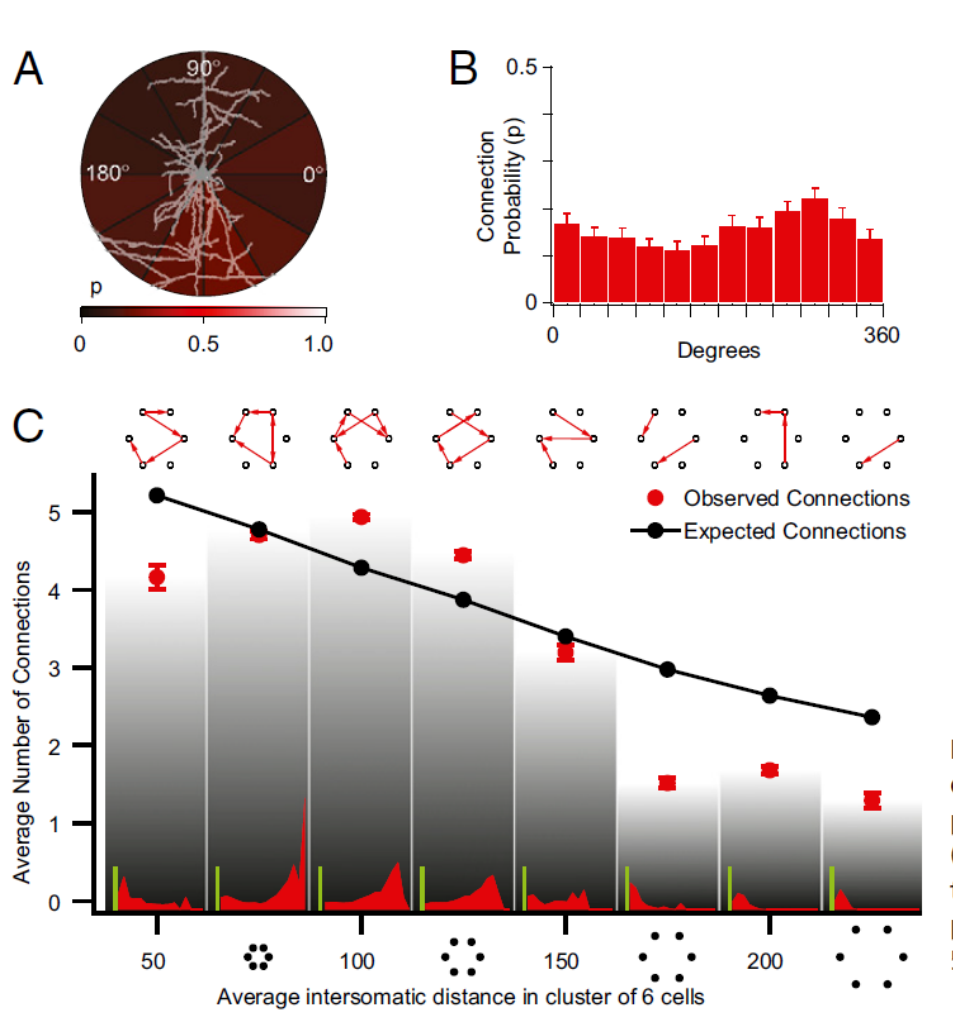


Fig. 1. Pair-wise connectivity. (*A*) Morphological staining of a cluster of 12 cells recorded simultaneously. (*B*) Region of the somatosensory cortex where recordings were carried out. (*C*) Connectivity diagram of neurons in *D*. (*D*) Example of recorded traces in an experimental session. A different neuron is stimulated and the responses of the remaining neurons were recorded (displayed in columns). [Scale bars: horizontal, 100 ms; vertical, 1 mV (15 mV for action potentials)]. (*E*–*G*) Connection probability profiles as a function of distance. Error bars represent SEM.



Significant differences in the overall distribution of the number of expected connections first appeared in groups containing six neurons (Fig. 2).

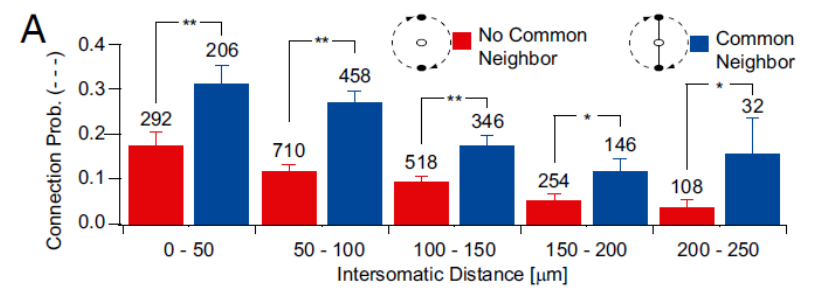
Fig. 2. Higher order connectivity. (*A*) Difference between the observed and expected values in *A* divided by the expected values [(observed – expected)/ expected]. (*Insets*) Schematic examples of possible patterns. Notice the increasingly larger disparity for clusters with many connections. (*B*) Comparison of observed (red) and expected (black) prevalence of given numbers of connections in clusters of three to eight cells. Error bars represent SEM.

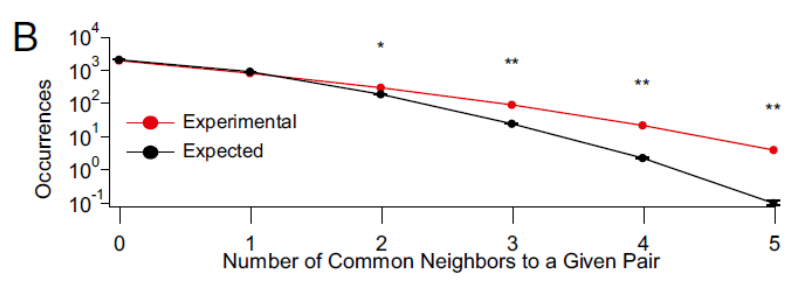


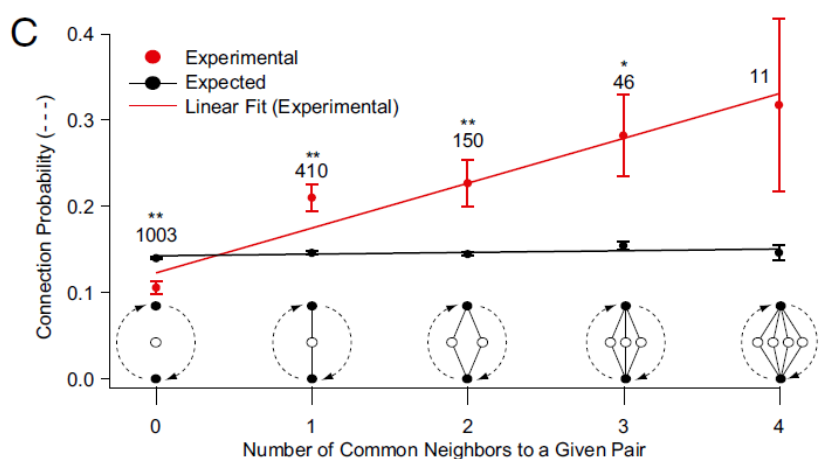
There was no significant correlation between the intersomatic orientation of the neurons and their connection probability (Fig. 3 A and B).

Multineuron patch-clamp recordings normally focus on neurons that are within about 50 μm of each other. We therefore searched for synaptic clustering over greater distances (up to 200 μm). Contrary to expectations, we found that the average number of connections in groups of six neurons initially increased rather than decreasing monotonically with mean intersomatic distance (Fig. 3C).

Fig. 3. Clustering. (*A*) Intensity plot of outgoing connection probability at different intersomatic orientations; brighter regions have higher connection probability. (*B*) Bar plot of connection probabilities at different orientations. (*C*) Average number of connections in clusters of six cells grouped according to cluster dimension. (*Insets*) Histograms of the difference over expected profiles as in Fig. 2*B* for different cluster dimensions. (Green scale bars value: 5.) Error bars represent SEM.







At any given distance, the connection probability for a pair of neurons with at least one common neighbor was significantly higher than the expected value (Fig. 4A) and that pairs of neurons sharing more than one common neighbor occurred significantly more often than expected (Fig. 4B). The connection probabilities rose linearly with the number of common neighbors (Fig. 4C).

Fig. 4. Common neighbor effect. (A) Connection probability as a function of distance comparing pairs that share a common neighbor against those that do not. (B) Occurrences of pairs of neurons sharing more than one common neighbor were significantly more numerous than expected by chance. (C) Connection probability between neurons as a function of the number of common neighbors experimentally observed. Error bars represent SEM.

Key points

- Use multi-patch clamp to study connectivity
- Example on how local connectivity deviates from random networks
- Introduce common neighbor bias
- Modeling is used to create random networks to compare with

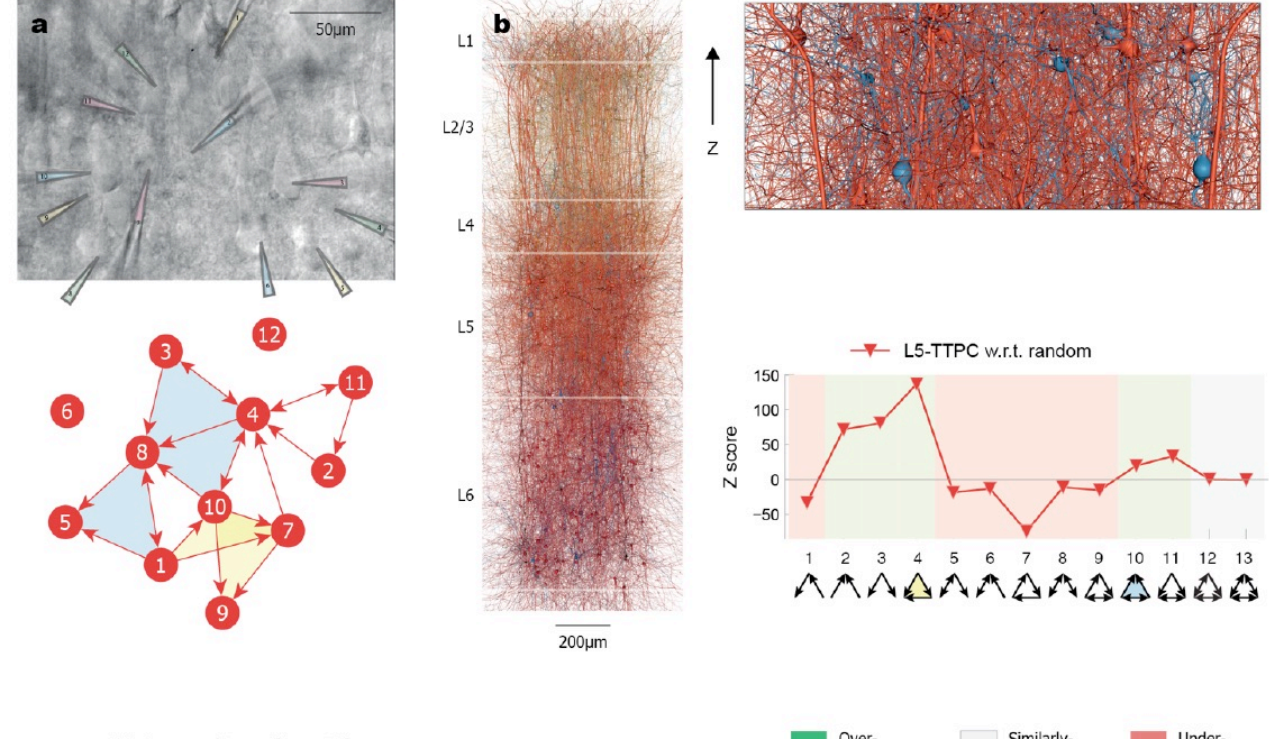


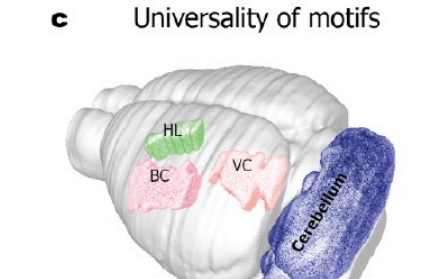
Neuron Geometry Underlies a Universal Local Architecture in Neuronal Networks

Eyal Gal¹, Rodrigo Perin², Henry Markram², Michael London^{1,3} and Idan Segev^{1,3}

¹The Edmond and Lily Safra Center for Brain Sciences, and ³Department of Neurobiology, The Hebrew University of Jerusalem, Jerusalem, Israel.

²Blue Brain Project, École Polytechnique Fédérale de Lausanne, Geneva, Switzerland





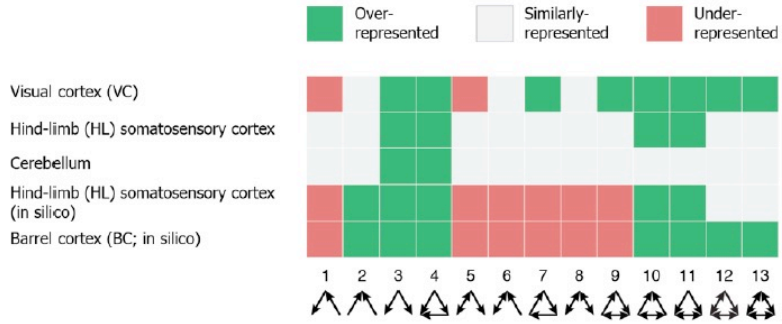


Figure 1. Universality of triplet motifs appearance in a variety of mammalian neuronal microcircuits.

a, Differential contrast video image of *in vitro* 12-patches recording from L5 thick tufted cortical pyramidal cells in rat somatosensory cortex (top). Triggering a spike in a presynaptic cell and recording excitatory post-synaptic synaptic potentials in the post-synaptic cells enabled to establish circuit connectivity diagram (schematically depicted at the bottom) and to count the frequencies of specific triplet motifs (two types of motifs are highlighted by light green and yellow). **b**, Left - dense *in silico* reconstruction of neocortical microcircuit (NMC) from the rat somatosensory cortex¹³; its volume is of ~0.3 mm³ with ~40 million synapses. Top right - a slice in L5 from the NMC circuit shown at left, with L5 thick tufted pyramidal cells (L5-TTPC) colored in red and L5 Martinotti cells (L5-MC) in blue. Lower frame - graph theoretical analysis of the connectivity diagrams for the two cell types shown above, highlighting the overrepresented triplet motifs (e.g., motifs #3 and #4), the underrepresented (e.g., motif # 7 for L5-TTPCs) ones, and those that are similarly represented, as compared to the respective distance-dependent random network (**Methods**). Triplet #4 is marked in yellow and triplet #10 in light blue, as in a, bottom. c, Universality of overrepresented triplet motifs in a variety of neuronal microcircuits. Note that triplets #3 and #4 are overrepresented in all circuits. The brain regions from which these microcircuits reside in is depicted schematically at left; the expression of the various triplet motifs in these circuits is shown at right. Triplet motifs expression data is displayed for primary visual cortex³; somatosensory cortex⁴; interneurons in the cerebellum⁵; dense *in silico* somato-sensory cortex¹⁴, and for dense *in silico* barrel cortex¹⁶.



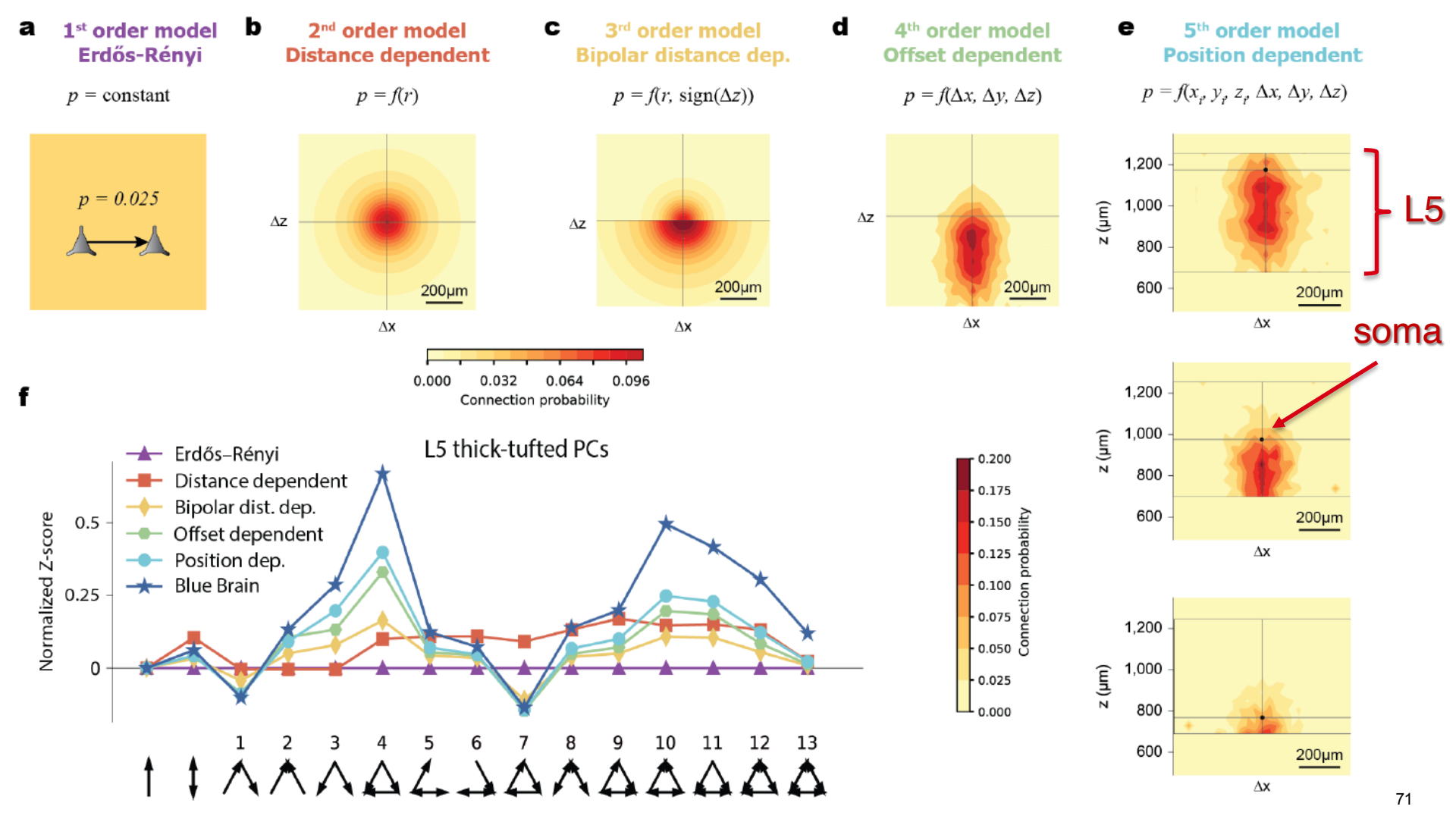


Figure 2. The anisotropic connectivity among cortical neurons and their spatial embedding in cortical volume underlie the emergence of triplet motifs in the NMC. a-e, a series of progressively more complex generative models for the circuit connectivity of L5 thick-tufted pyramidal cells (L5-TTPC). a, 1st order Erdős-Rényi model, with uniform connection probability, p = 0.025, among the cells as is the average connection probability in the NMC. **b**, 2^{nd} order model, in which p (color coded) is distance dependent, as derived from the NMC. p is depicted with respect to the distance from the postsynaptic cell located at the origin (Δx , Δz intersection point). Note the decrease in pwith distance. \mathbf{c} , 3rd order "bipolar" model, in which p also depends on whether the postsynaptic neuron is above or below the presynaptic cell (along the z-axis). Note that, in the NMC, p is larger for downwards connection. **d**, 4th order "offset dependent" model, in which p depends also on the relative direction, in 3D, to the postsynaptic cell as it does in the NMC. Note that p is larger for postsynaptic neurons that are directly below (along the z-axis), as compared to cells that are obliquely below the presynaptic cell. **e**, 5^{th} order model, in which p depends on the absolute position in 3D of both the presynaptic and the postsynaptic cells. E.g., L5-TTPCs whose somata are located close to the border of layer 4 (top horizontal line) have a larger span, in the z-direction, for having a postsynaptic partner as compared to L5-TTPCs whose somata reside near the border of layer 6 (bottom). **f**, Distribution of the various triplet motifs for each of the models shown in a-e, with respect to the reference Erdős-Rényi model (x-axis). Motifs distribution in the NMC is shown by the blue line. Note that, as the geometry captured by model becomes more realistic, their motifs appearance becomes closer to that of the NMC (blue line with stars). See Methods for detailed explanation regarding the construction of the different statistical models used in this figure.



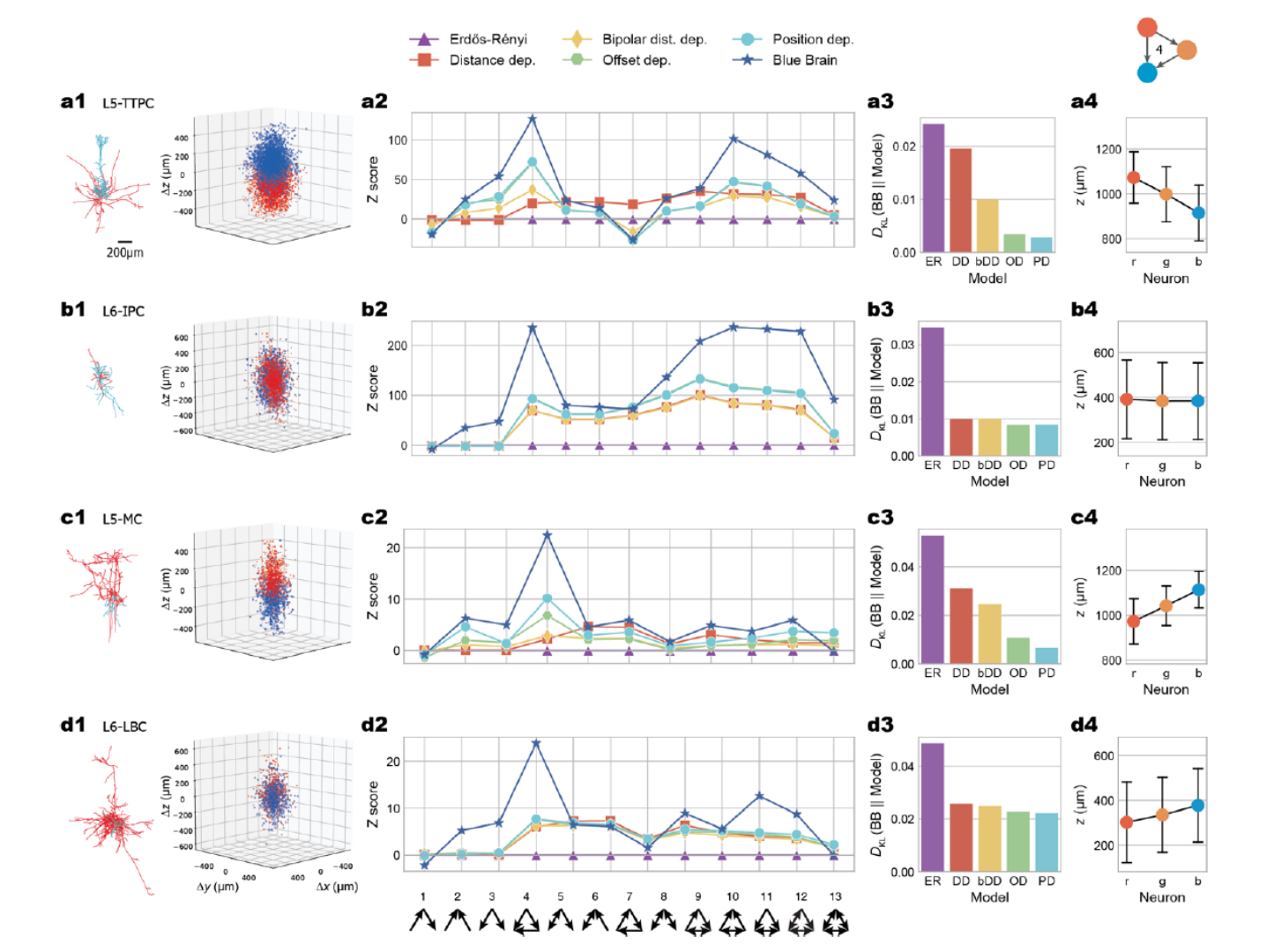


Figure 3. Impact of morphology of different cortical cell types on the emergence of triplet cell motifs in the NMC. **a**, Appearance of triplet motifs for L5-TTPC. **a1**, Left, an exemplar 3D reconstructed TTPC cell. Right, the relative soma position of all the presynaptic TTPC cells (blue) and all the postsynaptic TTPC cells (red) with respect to the cell somata centered at 0,0 (superposition of 50 TTPC cells). **a2**, Distribution of triplet motifs for TTPC cells (n=2,003). **a3**, Kullback—Leibler divergence between the motif distribution observed in the NMC and each of the 5 models shown in a2. Note the gradual improvement with model complexity. **A4**, spatial embedding of neurons composing motif #4 (mean ± s.d.). **b-d**, As in a, but for (**b**) L6 inverted pyramidal cells (n = 3,476), (**c**) L5 Martinotti cells (n=395) and (**d**) L6 large basket cells (n=463). Note that when the neuron is more isotropic as in **b** and **d**, models beyond the distance-dependent model do not provide further improvement.



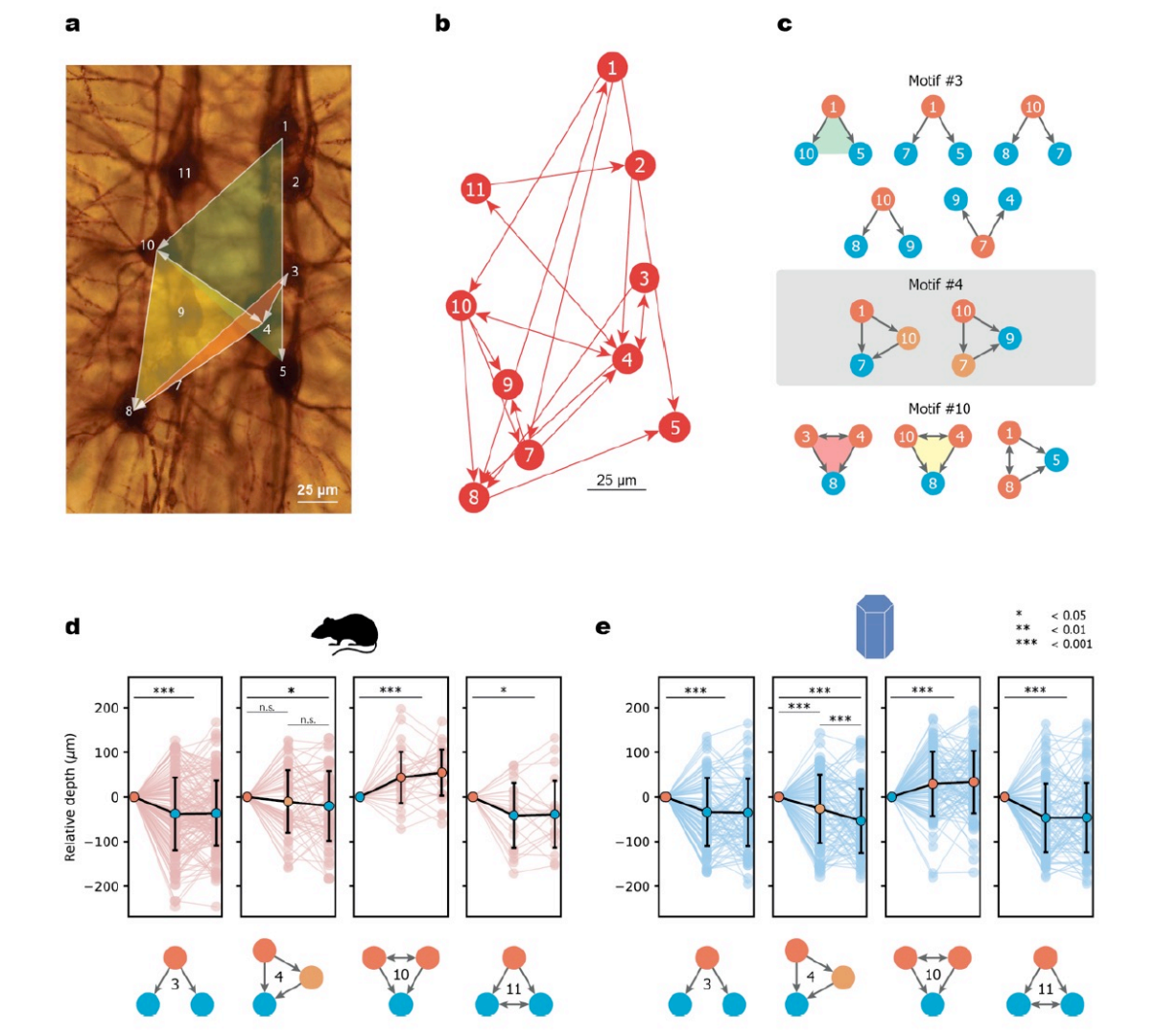




Figure 4. Experimental validation of motif spatial embedding. a, Biocytin staining of multi-patch recordings from 12 L5-TTPCs. Three exemplar connected triplet cells are shown by the transparent (green, yellow and red) triangles. **b**, Connectivity map for the 12-neurons circuit shown in a. **c**, All instances for three triplet motifs (#3, #4 and #10) that were extracted from the circuit diagram shown in b. The relative depth (z axis) of the cells composing these triplets is preserved. E.g., note that, for triplet #3, in most (but not in all) cases the presynaptic cell (red circle) is located above the two postsynaptic cells (blue circles). Green, yellow and pink triangles correspond to the respective cell triplets shown in a. **d**, Spatial embedding of triplet motifs (#3, #4, #10 and #11) for L5-TTPCs in the experimental data set (n_3 = 163, n_4 = 63, n_{10} = 31, n_{11} = 21 triplets); the relative depth of the cells forming individual triplets (light brown lines) and mean \pm s.d. (black line). For clarity, cell depths were aligned in each triplet according to one member (the left-most cell in the plot). *P < 0.05, **P < 0.01, ***P < 0.001. A paired-samples t-test. P values for R-vs-Y and Y-vs-B in motif #4 are 0.2470 and 0.3029, respectively. **e**, As in e but for a 400 μ m-thick slice from the NMC ($n_3 = 219,377, n_4 = 22,137$, $n_{10} = 833$ and $n_{11} = 765$ triplets of which only 100 instances are shown). Note the very close similarity between experiments (in e) and model (in d).



Key points

- Modeling offers full possibility in analysis
- A 'good' model has predictive power
- The model predicts that the divergence from random connectivity can be explained by a series of geometrical properties, first of all the anisotropy of morphologies
- This links back to the importance of morphologies
- We normally pass from experiments to models, in this paper we see an example on how useful is also to pass from models to experiments







Structured Synaptic Connectivity between Hippocampal Regions

Shaul Druckmann,^{1,5} Linqing Feng,^{2,5} Bokyoung Lee,^{2,3} Chaehyun Yook,^{2,4} Ting Zhao,¹ Jeffrey C. Magee,^{1,*} and Jinhyun Kim^{2,*}

¹Janelia Farm Research Campus, Howard Hughes Medical Institute, 19700 Helix Drive, Ashburn, Virginia 20147, USA

²Center for Functional Connectomics, Korea Institute of Science and Technology (KIST), 39-1 Hawolgokdong, Seoul, 136-791, Korea

³Neuroscience program, University of Science and Technology, 176 Gajeongdong, Daejeon, 305-350, Korea

⁴Department of Biological Science, KAIST, 373-1 Guseongdong, Daejeon, 305-701, Korea

⁵These authors contributed equally to this work

*Correspondence: mageej@janelia.hhmi.org (J.C.M.), kimj@kist.re.kr (J.K.)

http://dx.doi.org/10.1016/j.neuron.2013.11.026



mammalian GFP reconstitution across synaptic partners (mGRASP)

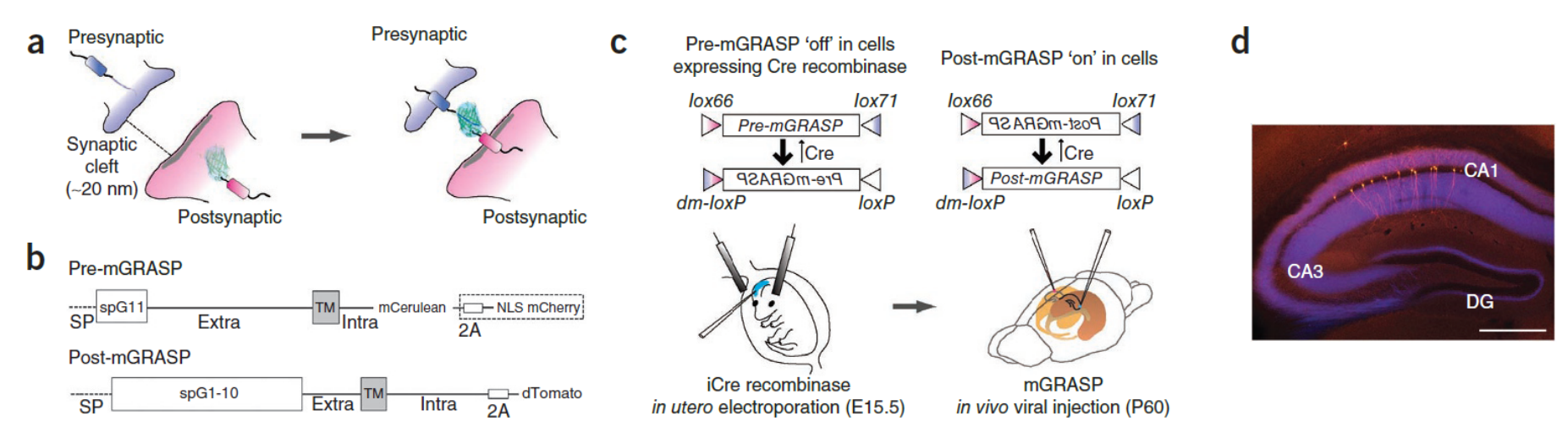


Figure 1 | Synaptic mGRASP components and gene-delivery strategy. (a) Schematic illustration of mGRASP in the synapse. (b) Diagram of pre- and post-mGRASP composed of signal peptide (SP), split-GFP fragment GFP1-10 (spG1-10) or GFP11 (spG11), extracellular domain (extra), transmembrane domain (TM) and intracellular domain (intra) followed by fluorescent proteins (mCerulean, 2A-mCherry or 2A-dTomato). (c) Strategy for cell-type-specific and sparse gene delivery. In addition to Cre recombinase-independent pre- and post-mGRASP, Cre recombinase-dependent 'switch off' pre-mGRASP and 'switch on' post-mGRASP were generated, by using two mutant *loxP* sites (*lox66* and *lox71*) in a head-to-head orientation. Because the double-mutated *loxP* (*dm-loxP*) site shows very low affinity for Cre recombinase and results in no or little inversion (indicated by up arrows), the favorable one-step inversion indicated by down arrows is nearly irreversible, allowing the gene to be stably switched 'on' and 'off' as desired. rAAV vectors for the expression of these constructs were injected into the hippocampus ~2 months after *in utero* electroporation of iCre recombinase on embryonic day 15.5 (E15.5) or into the hippocampus of Cre recombinase-expressing transgenic mice on postnatal day 60 (P60). (d) Example dTomato and mCerulean fluorescence merged image shows dense axonal projections of CA3 neurons infected with pre-mGRASP (*aavCAG-pre-mGRASP-mCerulean*; blue) and sparse CA1 pyramidal neurons expressing post-mGRASP (*aavCAG-Jx-rev-post-mGRASP-2A-dTomato*; red). Scale bar, 500 μm.

Kim et al., 2012

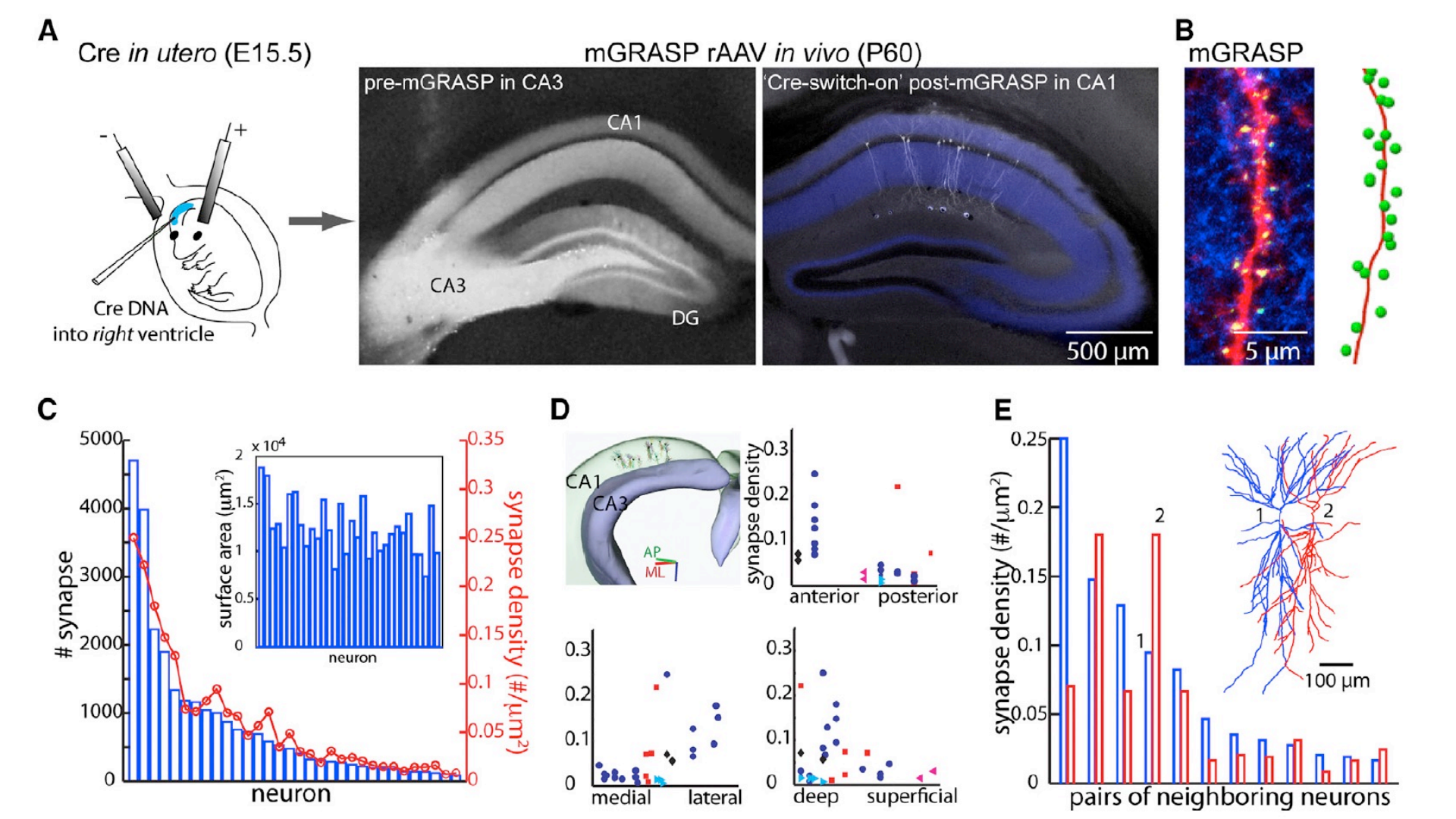
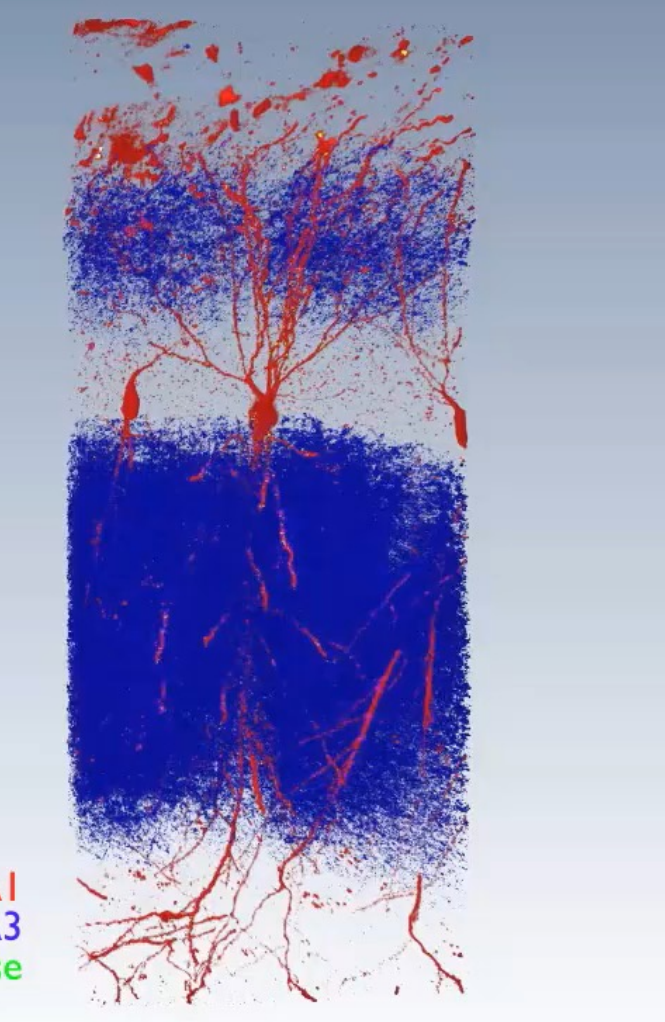


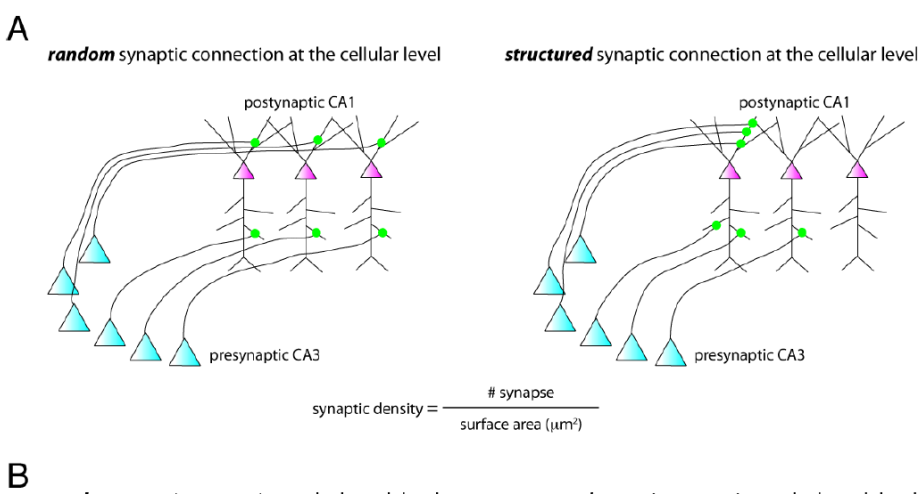
Figure 1. Variable Synaptic Connectivity at the Cellular Level

- (A) Strategy for mGRASP expression to study hippocampal CA3-CA1 synaptic connectivity pattern. Broad presynaptic CA3 and sparse postsynaptic CA1 labeling: the plasmid containing iCre recombinase was transfected into CA1 progenitor cells of the right ventricle via in utero electroporation on embryonic day 15.5 (E15.5). Cre-independent pre-mGRASP and Cre-dependent "switch on" post-mGRASP rAAV were injected into left CA3 and right CA1, respectively, on postnatal day 60~75. Example fluorescent images show dense axonal projection of CA3 neurons expressing pre-mGRASP (left) and sparse CA1 neurons expressing post-mGRASP in white along with dense CA3 axonal projections in blue (right).
- (B) Example dendrite showing a number of reconstituted mGRASP signals (green) in sites where dense CA3 axons (blue) intersect with a CA1 dendrite (red) (left) and its neuTube-reconstruction with detected mGRASP puncta (right).
- (C) Sorted bar plot shows highly variable number of synapses per neuron across population (828 \pm 1,065 [mean \pm STD], per neuron, range 83–4,701). Overlaid red graph indicates synaptic density and inset shows surface area of each neuron (surface area: 12,365 \pm 2,767 μ m², range 7,371–18,792; synaptic density: 0.061 \pm 0.06 synapse/ μ m², range 0.007–0.25).
- (D) Spatial location of postsynaptic CA1 neurons among 3D hippocampal landmarks (top left) and scatter plot of synaptic density versus spatial location. Different colors and markers indicate different animals. Anterior-posterior ranged $-2.0\sim-2.8$ mm from bregma (binned from 100- μ m-thick slices), medial-lateral ranged $1\sim2.25$ mm, and depth ranged $1\sim1.27$ mm from dura. AP: anterior-posterior, ML: medial-lateral.
- (E) Comparison of synaptic density of nearest-neighbor pairs in a single animal shows variable number of synapses per neuron within a single animal. The synaptic density of the first (blue) and second (red) neuron of the pair is shown, sorted by the density of the first pair member. Inset shows two neuTube-reconstructed neurons marked by 1, 2. See also Figure S1, Figure S2, and Movies S1, S2, and S3.

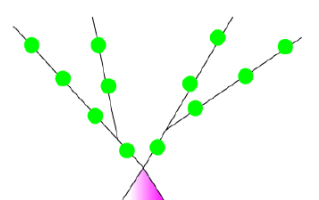




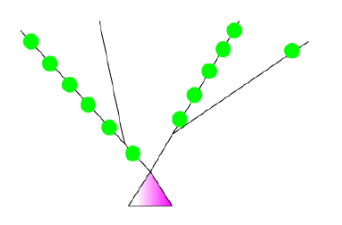
postsynaptic CAI presynaptic CA3 synapse



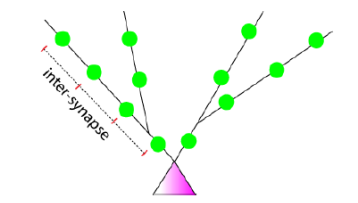




structured synaptic connection at the branch level



dispersed synaptic connection at the branch level



clustered synaptic connection at the branch level

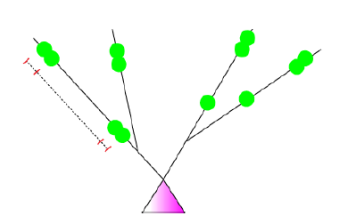




Figure S1. Synaptic distribution hypotheses. Related to Figure 1, 2, and 7.

A. Question: Do different neurons have different synaptic densities? Schematic diagrams represent random and selective synaptic connectivity patterns on postsynaptic neurons. This is tested by measuring the neuron-to-neuron variability in synaptic density when presynaptic neurons are broadly labeled by mGRASP. **B.** Question: Do different branches within one neuron have different densities? This is tested by measuring the branch-to-branch variability in synaptic density. **C.** Question: Are synapses on one branch distributed dispersed or clustered? This is tested by measuring the deviation from the expected exponential distribution of inter-synapse distances in broadly and selectively labeled data.



Key points

- Use of a combined technique to label axon, postsynaptic neurons, and synapses
- Long-range connectivity can also diverge from random networks
- This phenomenon can occur at different levels: inter-neurons, interbranches, intra-branch
- This behavior can really affect the communication from CA3 to CA1
- Connectivity patterns can be (quite) captured by axon-based approaches (Gal et al.), but the difficulty to have full-axon reconstructions complicates the modeling of long-range connectivity



Summary 3

- Experimental exploration of high-order connectivity is possible until a certain point, but it is showing the complexity of neuronal networks
- Both local and long-range connectivity show an high degree of complexity
- Each modeling approach capture a different portion of this complexity
- All three papers show a virtuous loop between experiments and models



Lecture Summary

- Connectome is a complex network that diverges significantly from random network
- Reconstructing the connectivity is a multi-scale problem
- Merging the scales is still challenging
- This is because techniques look at a smaller range of scales, techniques have a limited capability, we still lack of a complete understanding ...
- Modeling is a fundamental complementary tool to investigate connectivity because of the limitations of the techniques
- We start to understand the origin of this complexity
- And how much the different modeling approaches can approximate the real



What you have learnt

- Terminology (pathway, connection, bouton...)
- Connectivity matrix
- Calculate divergence, convergence...
- Higher-order connectivity patterns (local patterns, long-range topography, motifs...)
- Understand the different experimental techniques (light microscopy...)
- Understand the different modeling approaches (no volume, no axon...)

